International Journal of Engineering Science 133 (2018) 144–168

Contents lists available at ScienceDirect

International Journal of Engineering Science

journal homepage: www.elsevier.com/locate/ijengsci

Contact mechanics of a dilatant region located at a compressed elastic interface

A.P.S. Selvadurai[a,*], P.A. Selvadurai[b], A.P. Suvorov[c]

[a] Department of Civil Engineering and Applied Mechanics, McGill University, Montréal, QC H3A 0C3, Canada
[b] Department of Earth Sciences, Schweizerischer Erdbebendienst, ETH, Zürich 8092, Switzerland
[c] Department of Applied Mathematics, Moscow State University of Civil Engineering (MGSU), Moscow, Russia

ARTICLE INFO

Article history:
Received 6 July 2018
Revised 3 September 2018
Accepted 3 September 2018

Keywords:
Shear at an interface
Embedded dilatant patch
Evolution of normal stress with shear
Dilatancy degradation

ABSTRACT

Interfaces possess complex mechanical responses that are governed by several factors including the type of material, the local topography of the interacting surfaces, the stress state and the mode of deformation. This paper examines the mechanics of a mated smooth interface that is subjected to a normal stress and where the contact is perturbed by a circular patch that can experience dilatancy under shear. The analysis of the static stress drop occurring during shear at the interface is examined using a contact mechanics approach that accounts for the separation at the pre-compressed geological interface induced by the development of dilatancy of the patch during relative shear. This paper presents an elementary model of the mechanics that takes into consideration the normal stress evolution during dilatant shearing of the interface. The problem is of particular interest to the modelling of local phenomena that can occur at material interfaces and geological faults that are subjected to steady movement.

1. Introduction

The mechanical behaviour of geologic interfaces, particularly faults and fractures is important to several branches of engineering geosciences including stability of geologic strata, development of tectonic motion, displacements of pre-existing fractures and interaction of constructed underground facilities, where the interface behaviour is controlled by the stress state and the influence of both cohesive and frictional forces. The literature in this area is vast (nearly six thousand references covering the diverse areas of geomaterial interfaces, geologic fault zones, tribology, wear, biomechanics, contact mechanics, etc.) and no attempt will be made to provide a complete review of the subject. The historical studies related to mechanics of contact between surfaces date back to many scientists and engineers, including Leonardo da Vinci (1442–1519), Guillaume Amontons (1633–1705), John Theophilus Desaguliers (1683–1744), Leonhard Euler (1707–1783) and Charles Augustin de Coulomb (1736–1806) (see e.g., Hisano, 2018). The classical studies in mechanics of contact are also given by Bowden and Tabor (1986). Other contributions that emphasize engineering applications, mathematical modelling, computational modelling and experimental aspects of contact mechanics are given by Aleynikov (2011), Barber (2018), Curnier (1992), de Pater and Kalker (1975), Duvaut and Lions (1976), Galin (1961), Gladwell (1980), Johnson (1985), Kikuchi and Oden (1972), Klarbring, Mikelić, and Shillor (1991), Lur'e (1964), Michałowski and Mroz (1978), Panagiotopoulos (1989), Persson (2000), Raous, Jean, and Moreau (1995), Selvadurai (1979), Selvadurai and Atluri (2010), Ufliand (1965), Willner (2003) and

* Corresponding author.
E-mail address: patrick.selvadurai@mcgill.ca (A.P.S. Selvadurai).

https://doi.org/10.1016/j.ijengsci.2018.09.003
0020-7225/

others. Further references to problems in adhesive contact mechanics are also given in recent articles by Selvadurai and Katebi (2015) and Selvadurai (2016). The preceding articles also contain extensive references to computational aspects of contact mechanics and they can be supplemented by the volumes by Aliabadi and Brebbia (1993), Laursen (2003) and Wriggers and Laursen (2007).

The mechanics of geomaterial interfaces is reviewed in standard volumes and articles in geosciences, geomechanics and rock mechanics (Barton & Choubey, 1977; Barton and Stephansson, 1990; Ben-Zion and Sammis, 2010; Goodman & Dubois, 1972; Jaeger, 1971; Jaeger, Cook, & Zimmermann, 2007; Mogi, 1974; Nguyen & Selvadurai, 1998; Plesha, 1987; Rice & Cocco, 2007; Rossmanith, 1997; Scholz, 2002; Selvadurai and Boulon, 1995; Selvadurai and Voyiadjis, 1986). The articles by Plesha and Belytschko (1985), Rice and Ruina (1983), Ruina (1983), Selvadurai (1995), Selvadurai and Nguyen (1999), Selvadurai and Yu (2005), Zang and Stephansson (2010) and Pellet and Selvadurai (2016) have informative accounts of the mechanics of geological interfaces.

An early observation of dilatant processes with special reference to earthquake source mechanisms is due to Frank (1965). The poromechanical influences of dilatancy are also discussed by Brace and Martin (1968) and Nur (1972). The paper by Rice (1975) is an early attempt to include effects of poroelastic coupling on the dynamic stability of a dilatant interface. The article by Rudnicki and Chen (1988) also considers the stabilization of frictional slip on a weakening fault through dilatant and pore fluid pressure effects. The paper by Rice, Rudnicki, and Platt (2014) examines the stability and localization of a fluid-saturated gouge by developing a coupled thermo-hydro-mechanical approach (see also Selvadurai & Suvorov, 2016) with elastic and inelastic processes that can occur in a sub-region of a gouge layer. In the context of rupture at faults contributing to earthquakes, extensive reviews of the literature are also presented in recent articles by Selvadurai and Glaser (2015, 2017).

In this paper, we examine the idealized problem related to geomaterial halfspace regions in *smooth contact* and pre-compressed by a normal stress σ_0. The smooth interface is perturbed by a circular patch that possesses both *frictional* and *dilatant* mechanical properties. The Coulomb friction can be due to the contact at the local scale of the idealized Euclidean surfaces and dilatant effects can be due to surface irregularities. The dominant mechanism is asperity ride-up but the modelling presented here can account for the deterioration of the dilatancy angle that can be identified with asperity breakage and damage, indentation fracture (Michalowski, Zang, & Nadukuru, 2018; Selvadurai, 2000a), wear of the surfaces and gouge filling leading to slickenside features and wear. In the fields of tribology and materials science, wear functions have been used to describe the manner in which initially rough surfaces become smother in accordance with a polish-rate decay function (Archard, 1953; Borucki, 2002; Borucki, Witelski, Please, Kramer, & Schwendeman, 2004; Ciavarella, 2016). New findings (Siman-Tov, Aharanov, Boneh, & Reches, 2015) suggest that stressed natural geological fault planes experiencing relative shear can form mirror-like (smooth) surfaces. These mirror-like surfaces are believed to promote the localization of rupture in both the field (Goldberg, Siman-Tov, & Emmanuel, 2016) and laboratory simulations (Selvadurai, Edwards, Tormann, Wiemer, & Glaser, 2018), which provides a justification for considering in detail the micro-mechanical interactions at the contact zone. The research goal is to present a modelling approach that can capture, phenomenologically, the influences of dilatancy on the enhancement of the shear capacity of the contact zone. The problem can, of course, be examined using computational approaches that have been developed to examine frictional and dilatant contacts problems (Desai & Ma, 1992; Desai and Christian, 1975; Gens, Carol, & Alonso, 1995; Goodman & Dubois, 1972; Gudehus, 1977; Plesha & Belytschko, 1985; Plesha, Ballarini, & Parulekar, 1989; Selvadurai & Nguyen, 1999; Selvadurai & Yu, 2005; Zienkiewicz, Best, Dullage, & Stagg, 1970). The objective of this study is to develop a convenient analytical result that can be used to estimate the development of shear stresses at the frictional-dilatant circular patch during the relative shearing movement at the otherwise frictionless interface.

The problem posed here can be made quite complicated if the influence of the frictional contact at the entire surfaces of the fracture and the dilatant effects of the circular patch are considered simultaneously. Similar frictional “asperity” patches surrounded by frictionless or stress free regions have been considered in the literature (Anoosheshpoor & Brune, 2001; Beeler, Lockner, and Hickman, 2001; Chen & Sammis, 2003; Johnson & Nadeau, 2002; Sammis & Rice, 2001), and to the authors’ knowledge, the studies do not examine the possible influences of dilatancy, which forms the basis for the current study. We also endeavor to develop a theoretical approach to the study and it is unlikely that such a frictional contact problem will be amenable to an analytical treatment, and the approach adopted here is to examine the mechanics of the *dilatant circular patch during shear*, while maintaining frictionless behaviour of the exterior region of the interface. The justification for assuming frictionless behaviour exterior to the circular patch is to emphasize the constraint imposed by the dilatant patch and to evaluate the role of dilatancy at the patch in influencing the limiting shear capacity of the dilatant region. The presence of geofluids can also contribute to providing a frictionless state exterior to the dilatant patch. The frictional asperity model surrounded by a stress-free or frictionless (creeping) exterior region has been used to model asperity behaviour, specifically the physics surrounding repeating earthquakes on the San Andreas fault (Nadeau & Johnson, 1998). Repeating earthquakes (also known as repeaters) are frequently used to interpret local fault slip rates that help interpret bulk faulting behaviour (Kato, Igarashi, & Obara, 2014; Nadeau & McEvilly, 1999). We assume that the dilatant processes come into effect when the interface experiences a differential shear displacement in its plane. The dilatant movement is accommodated through the uniform displacement of the circular patch normal to its plane. The expansion can, of course, exhibit a variation over the circular region, but to preserve the simplicity of the model, we assume that the dilatant patch exerts a *uniform displacement* normal to its plane. This normal displacement can cause separation at the initially mated frictionless surfaces exterior to the circular patch, through its indentation into the deformable geologic media. The extent of separation

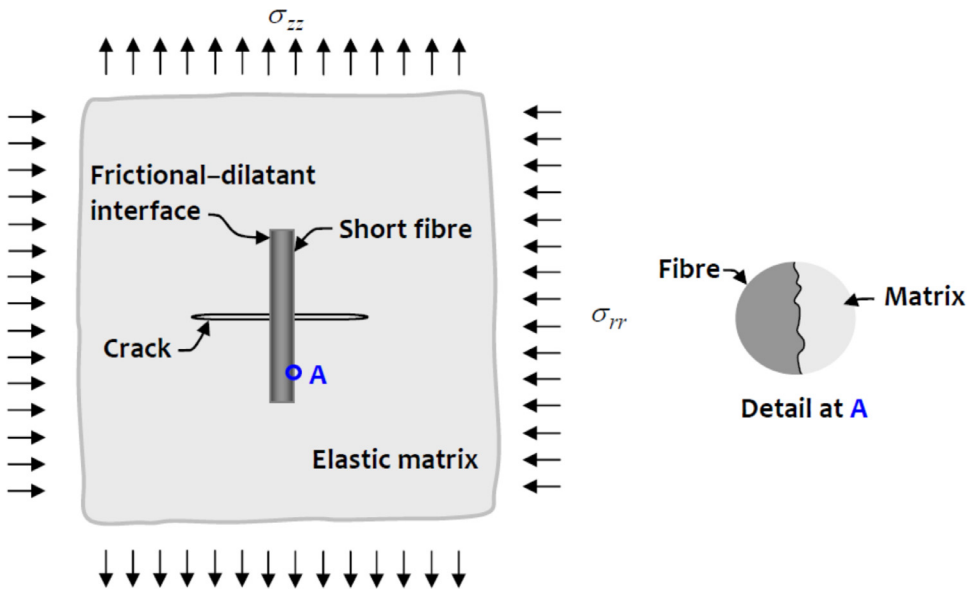

Fig. 1. Fibre-matrix interfaces exhibiting frictional-dilatant phenomena.

will depend on (i) the elasticity characteristics of the geologic material, (ii) the extent of dilatancy and (iii) the far-field normal stresses acting on the interacting surfaces. The paper presents an analysis of the elasticity problem associated with the dilatant patch and evaluates the normal stresses generated in the patch region during its dilatant expansion. This result is used in conjunction with a virtual work formulation to obtain a relationship for the shear stress at which the circular patch experiences failure or rupture.

Even though the primary motivation for the study is in relation to geological interfaces that can exhibit dilatant phenomena, the methodologies have a wide range of applications particularly in relation to materials and geological engineering in general. Consider for example composites that use short fibres in order to suppress the development and extension of cracks. The contact mechanics of the fibre-matrix interface can exert a significant influence on the stress intensity factors at bridged cracks (Fig. 1). A problem of matrix crack extension at a purely frictionally constrained bridging fiber was examined by Selvadurai (1994a, 2015) using a boundary element technique. The studies were restricted to an elasto-plastic interface exhibiting Coulomb friction. The methodologies can be extended to include fibre-matrix interfaces that possess dilatant frictional phenomena.

The topic of movement of large geological objects that can be triggered by earthquake action, chemical deterioration of the rock and other detrimental effects is of importance for the protection of human life and the environment. The movement of a dislodged boulder can result in a range of motions including free flight, rolling, sliding and impact (Fig. 2). The mechanics of boulder movement was examined by Turrin, Hanss, and Selvadurai (2009). In that treatment, the contact between the boulder and rock slope is restricted to Hertzian contact. The influence of Coulomb friction dilatant friction at contacting surfaces is expected to add another dimension to the analysis of rockfall simulation.

The application of discrete element techniques to the study of mechanics of granular materials is indiscriminate and ubiquitous. The prescription of contact between particles is largely achieved by appeal to Coulomb friction even though the particle surfaces have irregular topography that can contribute to processes such as finite friction and dilatancy. The contact conditions at particles can have a significant influence on overall mechanics of the granular medium and the inclusion of dilatant effects at contacts is considered to be an important extension to the realistic computational modelling of granular materials (Fig. 3).

The development of Tunnel Boring Machines (TBMs) have revolutionized the efficiency of construction of underground conduits used for transportation, power supply, water supply and waste water collection. The basic configuration of a TBM involves a rotary rock cutting face (Fig. 4) and conveyor systems for the efficient removal of excavated rock. The reaction necessary to apply the rock cutting forces is provided by hydraulic jacks that exert a normal radial stress at the interface between the TBM and the excavated tunnel. Conventional TBMs estimate the maximum reactive force by considering Coulomb friction at the interface. Estimate of the peak force, which in turn influences the excavation efficiency, can be improved by incorporating dilatant interfaces into the fabrication of the TBM reaction region.

Indentation tests are used extensively for the estimation of both fundamental properties of materials and for the validation of constitutive relationships applicable to materials. The conventional indentation tests involving either spherical or flat indenters generally assume frictionless contact between the indenter and the substrate. The influence of Coulomb friction and dilatant friction is expected to play a greater role when non-planar indenter surfaces are used in order to eliminate contact fracture (Selvadurai, 2000a) at locations of stress concentration associated with sharp edges (Fig. 5).

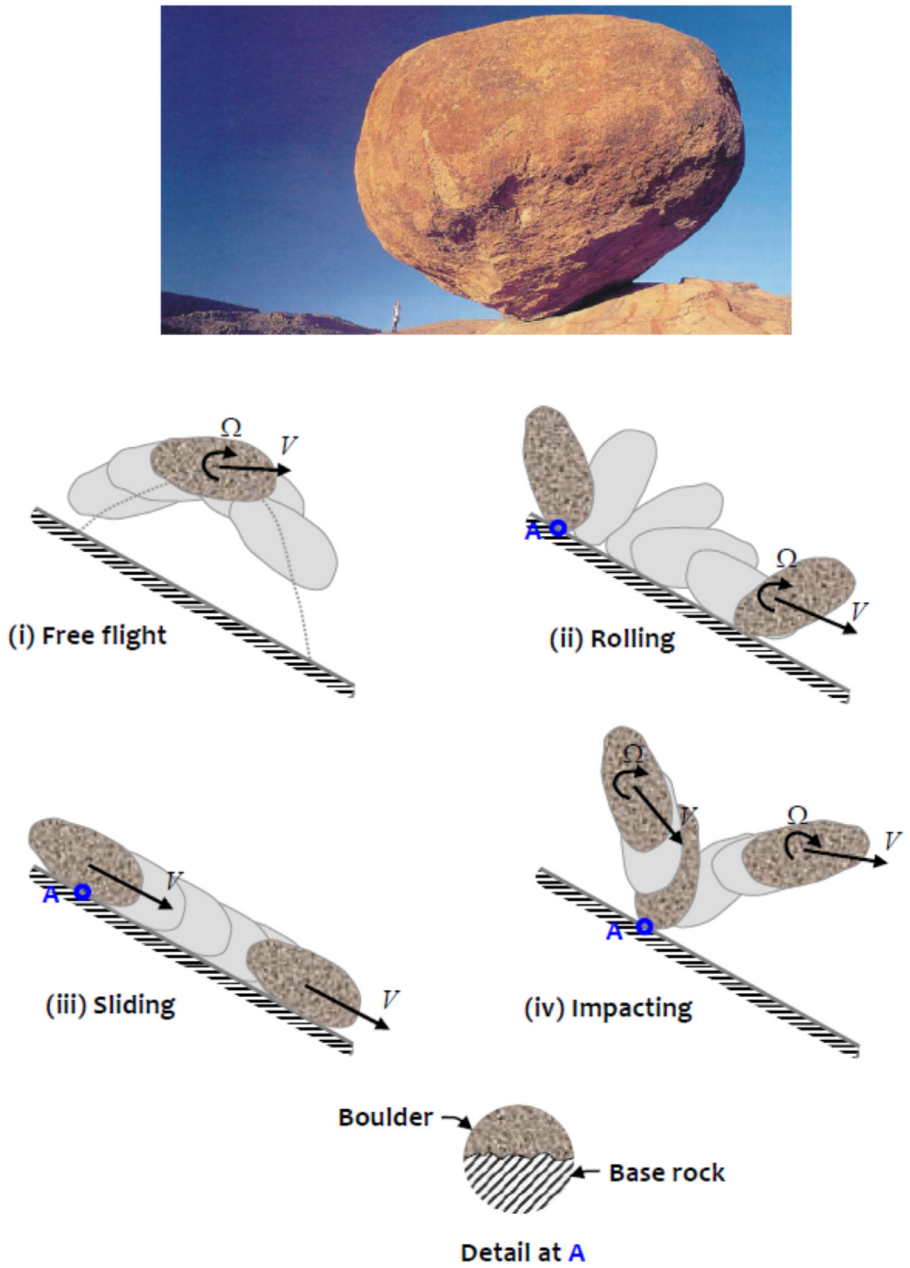

Fig. 2. The contact mechanics involving a dislodged boulder.

Indentation of flat membranes have also been used quite extensively for the study of hyperelastic materials including poly-vinyl chloride (Selvadurai & Yu, 2006) and hyperelastic rubber (Selvadurai, 2006). The deflected shape of the membrane provides a useful indicator for validation of the relevant constitutive theories. Fig. 6 shows the deflection pattern for PVC membranes subjected to indentation by a smooth spherical indenter. Fig. 7 shows analogous results for indentation of a hyperelastic membrane composed of natural gum rubber. The extension of the studies to include Coulomb friction and specifically dilatant friction can provide experimental data for validating both advanced computational approaches for non-classical contact conditions and constitutive theories.

2. Modelling of the elastostatic mechanics of the dilatant circular patch

We consider the problem of a frictionless contact between two halfspace regions under the action of a normal stress σ_0 and containing a frictional-dilatant circular patch (Fig. 8). The dilatant behaviour can be as a result of relative shearing

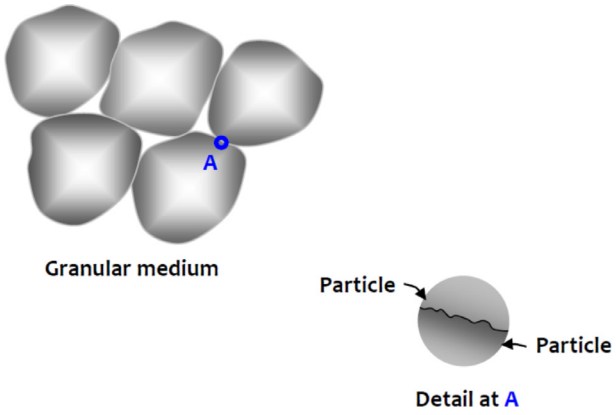

Fig. 3. Dilatant processes at particle contacts in granular media.

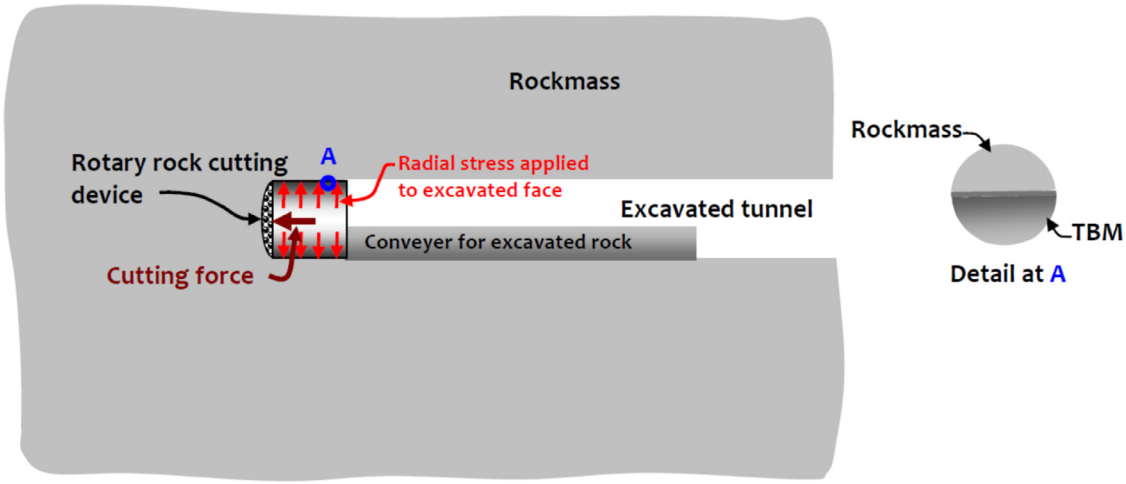

Fig. 4. Contact mechanics at the interface of a TBM.

action between the halfspace regions and in the process the dilation can result in an indentation orthogonal to the shearing displacements. We consider the elastostatic interaction between the frictionless interface containing the dilatant circular patch of radius a and consider the situation where the frictionless interface experiences a *total* relative movement $2\Delta u$ in its plane. (i) In general, the dilatancy-induced displacement normal to the circular patch can be variable within the dilatant region; for the purposes of developing convenient analytical result, we assume that the induced normal displacement at the frictional interface has a constant value Δv at both halfspace surfaces (Fig. 8). (ii) The dilatant behaviour of the circular patch will cause separation between the halfspace regions that are in smooth contact under the action of the compressive stress σ_0. (iii) The configuration of the boundary of the zone of separation can be elliptical in shape depending on the extent of shear. In this model, however, we assume that boundary of separation can be approximated by a circular profile of radius b, which is an unknown (Fig. 9) and needs to be determined by solving a unilateral contact problem for the two

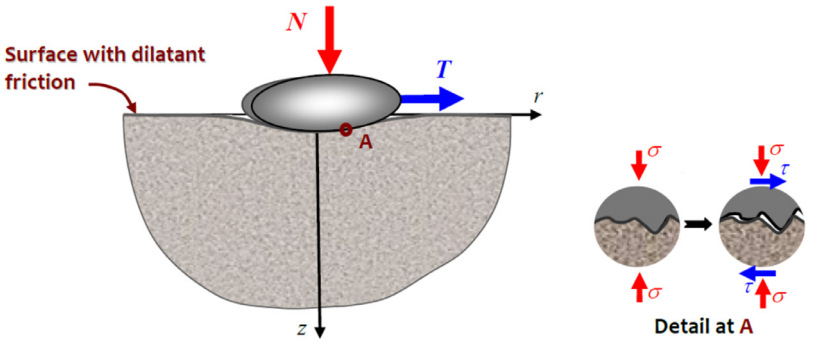

Fig. 5. Indentation tests involving indenter profiles without sharp edges.

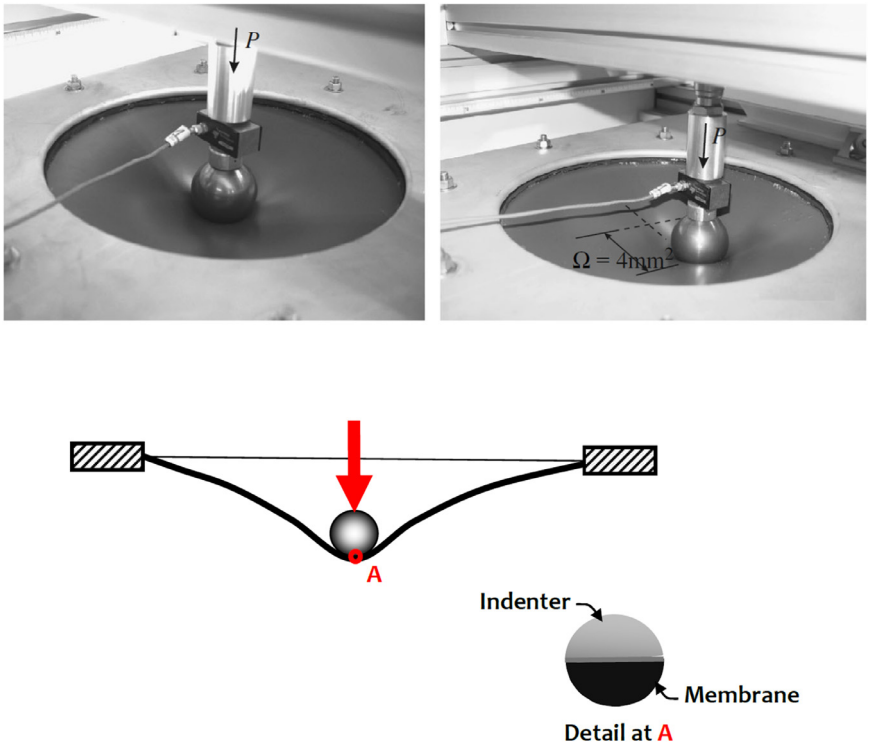

Fig. 6. Indentation of a PVC membrane by a smooth spherical indenter (Selvadurai & Yu, 2006).

halfspace regions. We emphasize the fact that contact regions, in general, have complex profiles that are neither planar nor axisymmetric. The overall methodology can, however, be extended to include other forms of contact regions (e.g., elliptical in particular) by adopting solutions to contact (Barber, 2018; Gladwell, 1980; Johnson, 1985; Lur'e, 1964) and crack problems with elliptical forms (Broberg, 1999; Cherepanov, 1978; Kachanov & Sevostianov, 2018; Kassir & Sih, 1975). The elliptical contact profile in particular, can be successfully used in conjunction with Galin's hypothesis (Galin, 1961) to "bound" the response of contact profiles with an arbitrary plan form.

The preliminary mathematical modelling of the dilatant shear rupture problem reduces to the analysis of the problem of two pre-compressed halfspace regions in smooth contact except over a circular region that experiences relative shear. The resulting elasticity problem is a three-dimensional *unilateral contact problem* (see e.g., Fichera, 1972; Gladwell, 1995; Gladwell & Hara, 1981; Selvadurai, 1980, 1994b, 1999, 2000b, 2003; Villaggio, 1980) where the boundary of the region of separation needs to be determined through an iterative scheme. The analysis of the problem can be considerably simplified by assuming that the shear-induced dilatant displacement is uniform over the shear zone and that the *zone of separation is nearly circular* (Selvadurai, 1980). This latter assumption converts the three-dimensional contact problem in elasticity to an axisymmetric contact problem. We need to develop a relationship between the force that is generated over the pre-compressed circular patch of radius a as a dilatant deformation that induces a uniform displacement Δv normal to its plane, which induces a zone of separation of finite radius b. The solution of the resulting axisymmetric problems in elasticity can

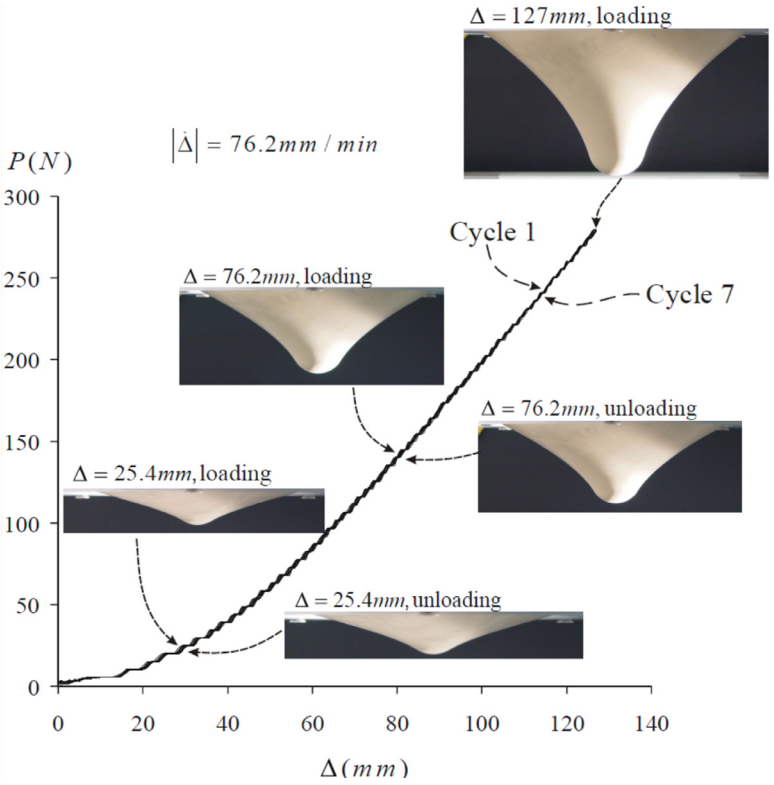

Fig. 7. Axisymmetric indentation of a hyperelastic membrane (Selvadurai, 2006).

be examined quite conveniently by using the strain potential approach of Love (1928) where, in the absence of body forces, the governing equation for the strain potential $\Phi(r,z)$satisfies the biharmonic equation

$$\nabla^2\nabla^2\Phi(r,z)=0 \tag{1}$$

where ∇^2 is the axisymmetric form of Laplace's operator in cylindrical polar coordinates. The displacements and stresses relevant to the formulation of the mixed boundary value problems that need to be examined in connection with the indentation and separation at the pre-compressed interface can be expressed in the following forms (Selvadurai, 2000c):

$$\begin{aligned} 2Gu_z(r,z) &= 2(1-\nu)\nabla^2\Phi - \tfrac{\partial^2\Phi}{\partial z^2} \\ \sigma_{zz}(r,z) &= \tfrac{\partial}{\partial z}\left\{(2-\nu)\nabla^2\Phi - \tfrac{\partial^2\Phi}{\partial z^2}\right\} \\ \sigma_{rz}(r,z) &= \tfrac{\partial}{\partial r}\left\{(1-\nu)\nabla^2\Phi - \tfrac{\partial^2\Phi}{\partial z^2}\right\} \end{aligned} \tag{2}$$

In the context of the contact problems, solution of (1) relevant to semi-infinite domains requires that during application of traction and displacements fields to the surface of halfspace regions, with $r\in(0,\infty)$ and $z\in(0,\infty)$, the displacements and stresses in halfspace regions should uniformly vanish as $(r,z)\to\infty$. The relevant solution can be written as

$$\Phi(r,z)=\int_0^\infty \{A(\xi)+zB(\xi)\}\,e^{-\xi z}J_0(\xi r)\,d\xi \tag{3}$$

where $A(\xi)$and $B(\xi)$ are arbitrary functions to be determined by satisfying the traction and displacement boundary conditions applicable to the relevant contact problem. For the analysis of the unilateral contact problem resulting from the indentation of the interface, we utilize the following two problems.

2.1. Auxiliary Problem I

We consider the frictionless indentation of a penny-shaped crack of radius b by a rigid smooth indenter of radius a and thickness $2\Delta\nu$ (Fig. 10). The associated problem in elasticity can be posed as a mixed boundary value problem related to a halfspace region, the surface of which is subjected to the mixed boundary conditions

$$\begin{aligned} &\sigma_{rz}(r,0)=0 \quad ; \quad r\geq 0 \\ &u_z(r,0)=\Delta\nu \quad ; \quad 0\leq r\leq a \\ &\sigma_{zz}(r,0)=0 \quad ; \quad a<r<b \\ &u_z(r,0)=0 \quad ; \quad b\leq r<\infty \end{aligned} \tag{4}$$

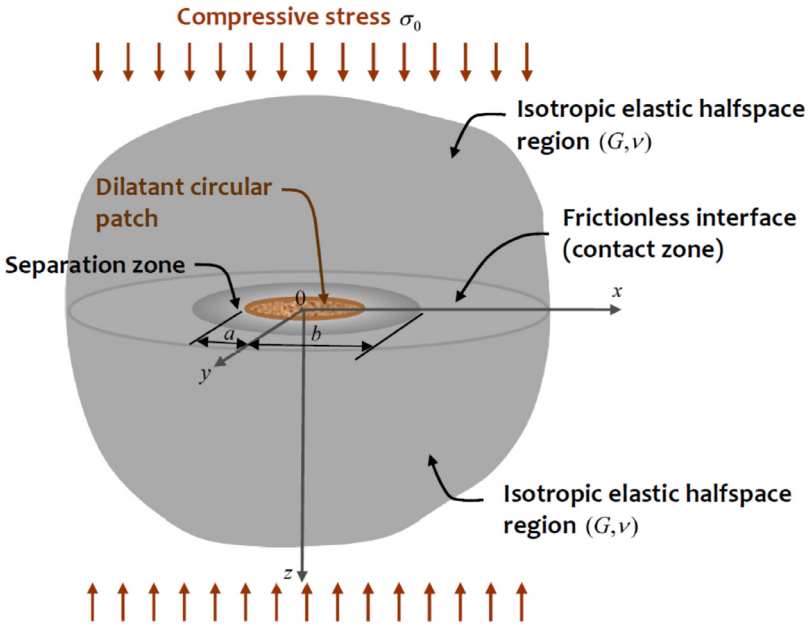

Fig. 8. Geometry of the dilatant patch problem.

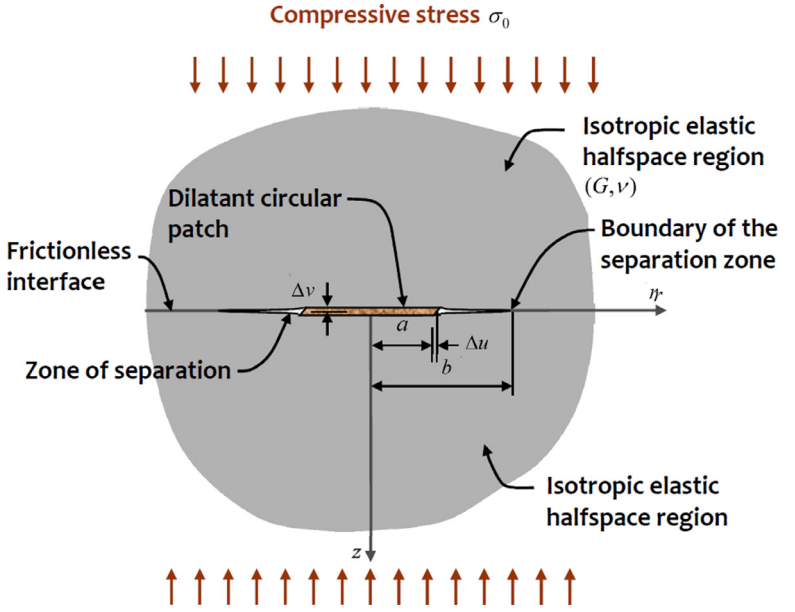

Fig. 9. Indentation of the halfspace regions by the dilatant displacements induced during shearing of the circular patch.

Using (2) and (3), the boundary conditions (4) can be reduced to a system of triple integral equations for a single unknown function $R(\xi)$ of the form

$$\begin{aligned}
&\int_0^\infty \xi^{-1} R(\xi) J_0(\xi r)\, d\xi = -\frac{G\Delta v}{(1-\nu)} \quad ; \quad 0 \le r \le a \\
&\int_0^\infty R(\xi) J_0(\xi r)\, d\xi = 0 \qquad\qquad ; \quad a < r < b \\
&\int_0^\infty \xi^{-1} R(\xi) J_0(\xi r)\, d\xi = 0 \qquad\qquad ; \quad b \le r < \infty
\end{aligned} \tag{5}$$

To the authors' knowledge, the system of triple integral equations (5) has no known exact solution. Methods for their solution in an approximate form are given by Tranter (1960), Cooke (1963), Williams (1963), Sneddon (1966) and

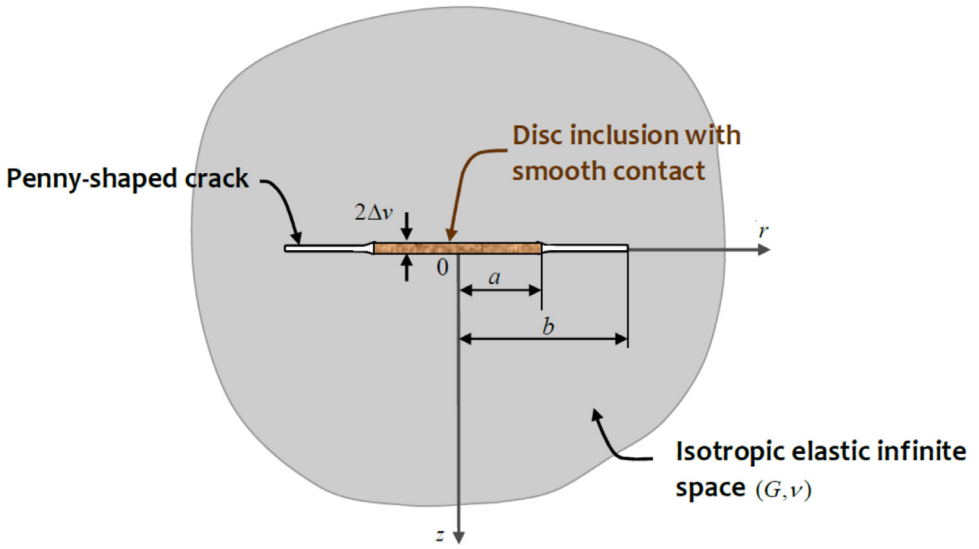

Fig. 10. Auxiliary Problem I: the indentation of a penny-shaped crack by a smooth rigid disc inclusion of thickness $2\Delta v$.

Kanwal (1971). The solution procedure proposed by Selvadurai and Singh (1984) involves the reduction of the system (5) to a single *Fredholm integral equation of the second-kind*, of the form

$$\Psi(\eta) = 1 + \int_0^1 \Psi(\omega) K(\omega, \eta)\, d\omega \quad ; \quad 0 \le \eta \le 1 \tag{6}$$

for a function $\Psi(\eta)$, which is related to $R(\xi)$, where the kernel function is given by

$$K(\omega, \eta) = -\frac{2\omega(1 - c^2\omega^2)^{1/2}}{\pi^2(1 - \omega^2)^{1/2}}\left(\frac{\Omega(\omega) - \Omega(\eta)}{\omega^2 - \eta^2}\right)$$
$$\Omega(\alpha) = \tau \ln\left\{\frac{1 + c\tau}{1 - c\tau}\right\} \quad ; \quad \tau = \left(\frac{1 - \alpha^2}{1 - c^2\alpha^2}\right)^{1/2} \quad ; \quad (\alpha = \omega, \eta) \tag{7}$$

and $c = a/b$. The method of solution is a development of a series approximation solution of (6) in terms of the non-dimensional parameter $c < 1$. The results of interest to the analysis of the *shear rupture problem* are (i) the contact force generated at the indentation zone and (ii) the Mode I stress intensity factor at the boundary of the penny-shaped crack, which can also be expressed as a series in terms of the parameter c. The force $P_{\Delta v}$ generated at the contact zone due to the indentation can be evaluated in the form

$$P_{\Delta v} = 2\pi \int_0^a r\sigma_{zz}(r, 0)dr = \frac{4aG\Delta v}{(1 - \nu)}\left[\begin{array}{l}\left(1 + \frac{4c}{\pi}\right) + \frac{16c^2}{\pi^4} + c^3\left(\frac{64}{\pi^6} + \frac{16}{9\pi^4} - \frac{8}{9\pi^2}\right) \\ +c^4\left(\frac{256}{\pi^8} + \frac{64}{9\pi^4}\right) + c^5\left(\frac{10240}{\pi^{10}} + \frac{9600}{225\pi^6} + \frac{92}{225\pi^2}\right)\end{array}\right] \tag{8}$$

where the series expansion solution is valid to $O(c^6)$. Similarly, the Mode I stress intensity factor at the boundary of the penny-shaped crack can be evaluated in the form

$$K_I^{\Delta v} = \frac{G\Delta v}{\pi(1 - \nu)\sqrt{b}} F_{\Delta v}(c) \tag{9}$$

where

$$F_{\Delta v}(c) = \left[\begin{array}{l}\frac{4c}{\pi} + \frac{16c^2}{\pi^3} + c^3\left(\frac{64}{\pi^5} + \frac{4}{3\pi}\right) \\ +c^4\left(\frac{80}{9\pi^3} + \frac{256}{\pi^7}\right) + c^5\left(\frac{448}{9\pi^5} + \frac{1024}{\pi^9} + \frac{4}{5\pi}\right)\end{array}\right] \tag{10}$$

The accuracy of the series approximation solution for the stress intensity factor has also been verified through comparisons with a quadrature scheme based solutions of (6) (Selvadurai, 1985).

2.2. Auxiliary Problem II

We next consider the internal pressurization by a compressive stress σ_0 (Fig. 11) of an annular crack with an inner radius a and an outer radius b located in an elastic medium of infinite extent. The mixed boundary value problem associated with

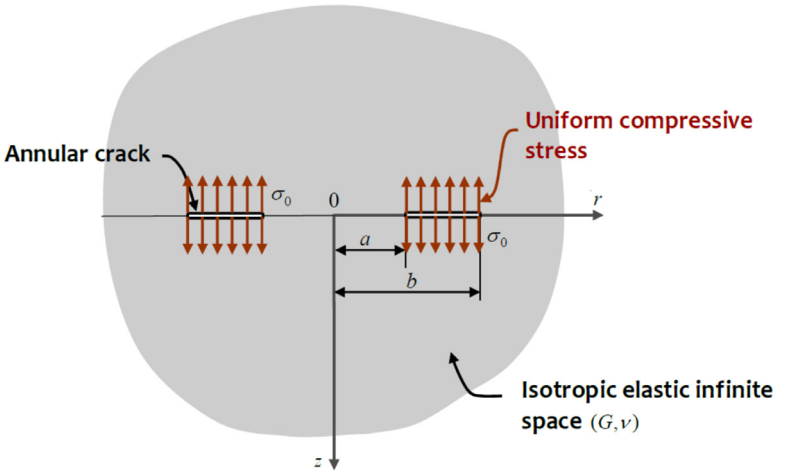

Fig. 11. Auxiliary Problem II: the internal pressurization of an annular crack by a uniform compressive stress σ_0.

the pressurization of the annular region can also be formulated as a mixed boundary value problem related to a halfspace region $0 \le r < \infty$ and $0 \le z < \infty$ and the relevant boundary conditions are

$$\begin{aligned} &\sigma_{rz}(r,0) = 0 \quad ; \quad r \ge 0 \\ &u_z(r,0) = 0 \quad ; \quad 0 \le r \le a \\ &\sigma_{zz}(r,0) = -\sigma_0 \quad ; \quad a < r < b \\ &u_z(r,0) = 0 \quad ; \quad b \le r < \infty \end{aligned} \tag{11}$$

The mixed boundary conditions (11) can also be reduced to a system of triple integral equations of the form

$$\begin{aligned} &\textstyle\int_0^\infty S(\xi) J_0(\xi r)\, d\xi = 0; \qquad 0 \le r \le a \\ &\textstyle\int_0^\infty \xi S(\xi) J_0(\xi r)\, d\xi = -\sigma_0; \quad a < r < b \\ &\textstyle\int_0^\infty S(\xi) J_0(\xi r)\, d\xi = 0; \qquad b \le r < \infty \end{aligned} \tag{12}$$

for the single unknown function $S(\xi)$. The method of solution of the system of triple integral equations (12) is along the lines discussed previously and the procedures have been used effectively to examine the mechanics of annular cracks (Selvadurai & Singh, 1985). The results of interest to the shear rupture modelling problem are the resultant force generated in the region $0 < r < a$ and the Mode I stress intensity factor at the outer periphery of the annular crack. Here again, the method of solution involves developing the results in power series in terms of the non-dimensional parameter $c(= a/b) < 1$. The force generated at the central bridging or intact region can be expressed in the form

$$\begin{aligned} P_{\sigma_0} &= 2\pi \textstyle\int_0^a \sigma_{zz}(r) r dr \\ &= \sigma_0 \pi a^2 \left(\begin{array}{l} -\dfrac{8}{\pi^2 c} + \left\{1 - \dfrac{32}{\pi^4}\right\} + 8c\left\{\dfrac{1}{\pi^2} - \dfrac{48}{\pi^6}\right\} \\ -\dfrac{c^2}{9\pi^8}\left\{4608 + \pi^3\left(32 - 64\pi + 3\pi^3\right)\right\} \\ -\dfrac{4c^3}{45\pi^{10}}\left\{23040 + \pi^3\left(-320 + 480\pi + 15\pi^3 + 6\pi^5\right)\right\} \\ -\dfrac{c^4}{675\pi^{12}}\left\{ \begin{array}{l} 5529600 + \\ \pi^3\left(-76800 + \pi\left[\begin{array}{l} 192000 \\ +\pi^2\left(3600 + \pi\left\{-320 + 3168\pi + 45\pi^3\right\}\right) \end{array}\right]\right) \end{array}\right\} \end{array}\right) \end{aligned} \tag{13}$$

We note that although the expression (13) is given to $O(c^4)$, the results are consistent with the corresponding expression (8) derived in connection with the indentation. Similarly, the Mode I stress intensity factor at the external boundary of the annular shaped crack can be evaluated in the form

$$K_I^{\sigma_0} = \frac{2\sigma_0\sqrt{b}}{\pi} F_{\sigma_0}(c) \tag{14}$$

where

$$F_{\sigma_0}(c) = \left[\begin{array}{l} 1 - \dfrac{4c}{\pi^2} - \dfrac{16c^2}{\pi^4} - c^3\left(\dfrac{1}{8} + \dfrac{64}{\pi^6}\right) \\ -c^4\left\{\dfrac{16}{3\pi^4} + \dfrac{4}{\pi^2}\left(\dfrac{1}{24} - \dfrac{8}{9\pi^2} + \dfrac{64}{\pi^6} + \dfrac{4}{9\pi^3}\right)\right\} \\ -c^5\left\{\dfrac{16}{\pi^4}\left(\dfrac{1}{24} - \dfrac{8}{9\pi^3} + \dfrac{64}{\pi^6} + \dfrac{8}{9\pi^2}\right) + \dfrac{256}{9\pi^6} - \dfrac{4}{15\pi^2}\right\} + O(c^6) \end{array}\right] \tag{15}$$

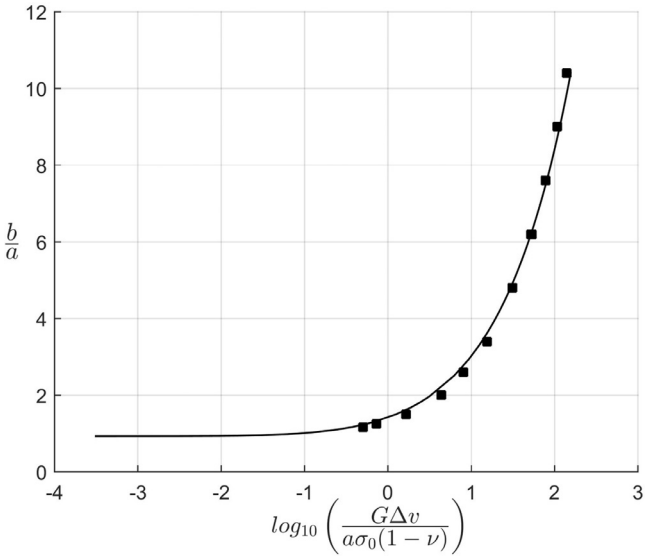

Fig. 12. The influence of the pre-compression stress σ_0 and the dilatancy induced displacement Δv on the radius of the zone of separation. [Solid line corresponds to the analytical estimate and the squares correspond to the computational results. Note that $c = a/b < 1$.]

We note that the radius b ultimately represents the radius of the circle of separation between the pre-compressed halfspace regions due to the indentation of each halfspace region by Δv. The analysis of these auxiliary problems can be used to evaluate the radius of the zone of separation. The basic assumption for determining b assumes that at the circle of separation, the contact stress reduces uniformly to zero and the surfaces of the separation zone are traction free. This can be interpreted as the vanishing of the Mode I stress intensity factor at $r = b$. The solution for the internal pressurization in the Auxiliary Problem II involves a compressive stress σ_0. In order to render the surfaces of the separated regions traction free, the stress that is applied to the annular region in the Auxiliary Problem II should be tensile with the proviso that, physically, the boundaries of the annular crack remain in an open condition to generate a Mode I stress intensity factor. This involves a change in the sign of the applied stress σ_0, when using (14), which gives a characteristic equation of the form

$$\left(\frac{G\Delta v}{2\sigma_0 a(1-\nu)}\right) cF_{\Delta v}(c) - F_{\sigma_0}(c) = 0 \tag{16}$$

This equation can be solved to determine the radius of the zone of separation due to the dilatancy-induced uniform indentation Δv over the region $0 \le r \le a$ of the interface composed of elastic halfspace regions (G, ν) subject to a pre-compression σ_0. The lowest positive root of (16) gives the radius of the separation zone. It should be remarked that the resulting value for the radius of the separation zone is an analytically derived result that uses a series expansion technique in terms of $c < 1$. It could be visualized that as the non-dimensional pre-compression σ_0/G increases, the zone of separation will decrease and $c \to 1$, and the result from the series expansion-based analytical approach will not be entirely accurate. To assess the limits of applicability of the estimation of the separation zone, the separation zone was evaluated using the finite element (FE) scheme available in the general purpose FE code ABAQUS^{TM}. Both the penalty function and augmented Lagrangian techniques have been used, as a constraint enforcement method, for the computational simulations. Fig. 12 illustrates a comparison between the analytical and computational results obtained for the zone of separation. There is good correlation between the analytical and computational results for a wide range of the non-dimensional parameter $G\Delta v/a\sigma_0(1-\nu)$ that incorporates the influences of the normalized pre-compressive stress σ_0/G and the normalized dilatancy-induced indentation $\Delta v/a$. As either the non-dimensional indentation $(\Delta v/a) \to 0$, or as the non-dimensional pre-compression $(\sigma_0/G) \to \infty$, the ratio $(a/b) \to 1$. The analytical results and the computational estimates give consistent estimates and trends.

2.3. Axial force induced by the indentation

The additional result that is required for the analysis of the shear rupture of the circular region undergoing dilatancy relates to the force that is generated on the indenting region. This result can also be expressed as an analytical expression in terms of the non-dimensional parameter $c < 1$. The result is composed of the resultant of contact stresses generated from the problem of the internal indentation of the penny-shaped crack given by (8), the resultant of stresses in the bridging region of the annular crack $0 < r < a$ given by (13) (with the sign appropriately adjusted to reflect the tensile tractions in the annular region) and the stresses applied through the far field pre-compression stress σ_0 Omitting the details it can be

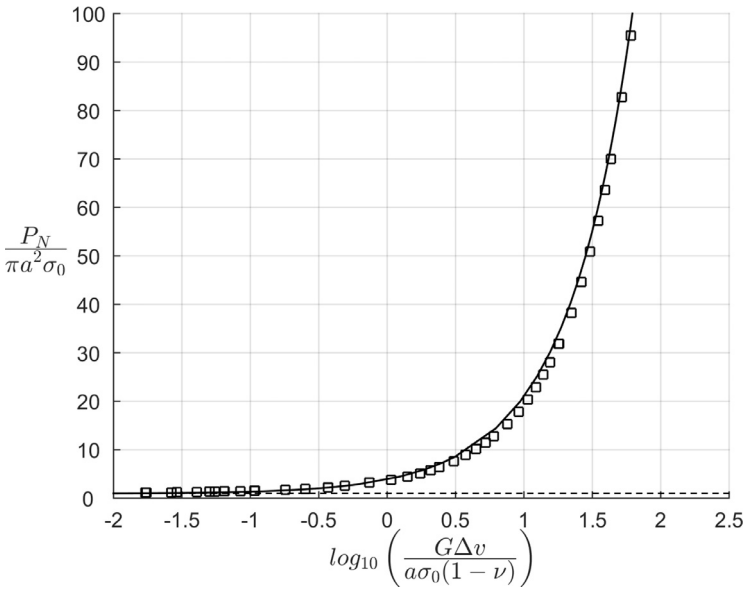

Fig. 13. The semi-log variation in the normalized force $(P_N/\pi a^2\sigma_0)$ generated in the indentation zone as a function of the normalized indentation-precompression parameter $\{G\Delta v/a\sigma_0(1-\nu)\}$. [Solid line corresponds to the analytical estimate and the squares correspond to the computational results.]

shown that the force generated at the contact zone of the indenting region $0 \le r \le a$, with a separation region $a \le r \le b$ and a re-established contact zone $b \le r \le \infty$, can be evaluated in the form

$$P_N = \sigma_0 \pi a^2 + \frac{4aG\Delta v}{(1-\nu)} P_N^{\Delta v} - \sigma_0 \pi a^2 P_N^{\sigma_0} \tag{17}$$

where

$$P_N^{\Delta v} = \left[\begin{array}{l} \left(1 + \dfrac{4c}{\pi}\right) + \dfrac{16c^2}{\pi^4} + c^3\left(\dfrac{64}{\pi^6} + \dfrac{16}{9\pi^4} - \dfrac{8}{9\pi^2}\right) \\ +c^4\left(\dfrac{256}{\pi^8} + \dfrac{64}{9\pi^4}\right) + c^5\left(\dfrac{10240}{\pi^{10}} + \dfrac{9600}{225\pi^6} + \dfrac{92}{225\pi^2}\right) \end{array} \right] \tag{18}$$

$$P_N^{\sigma_0} = \left(\begin{array}{l} -\dfrac{8}{\pi^2 c} + \left\{1 - \dfrac{32}{\pi^4}\right\} + 8c\left\{\dfrac{1}{\pi^2} - \dfrac{48}{\pi^6}\right\} \\ -\dfrac{c^2}{9\pi^8}\left\{4608 + \pi^3\left(32 - 64\pi + 3\pi^3\right)\right\} \\ -\dfrac{4c^3}{45\pi^{10}}\left\{23040 + \pi^3\left(-320 + 480\pi + 15\pi^3 + 6\pi^5\right)\right\} \\ -\dfrac{c^4}{675\pi^{12}}\left\{5529600 + \pi^3\left(-76800 + \pi\left[\begin{array}{l} 192000 \\ +\pi^2\left(3600 + \pi\left\{-320 + 3168\pi + 45\pi^3\right\}\right) \end{array}\right]\right)\right\} \end{array} \right) \tag{19}$$

Again, it is important emphasize that the analytical expression (17) is a convenient approximation to the force generated at the indentation zone valid for $c < 1$. We note that when indentation takes place in the absence of a pre-compression $\sigma_0 = 0$, $c(= a/b) \to 0$ and (17) reduces to the result for the force-displacement relationship given by Boussinesq (1885) (see also Harding & Sneddon, 1945; Davis & Selvadurai, 1996) for the indentation of the surface of a halfspace by a smooth rigid indenter and can be given in the form

$$P_N = \frac{4aG\Delta v}{(1-\nu)}. \tag{20}$$

As a check on the accuracy of the approximate analytical result (17), we also develop a computational result based on a finite element modelling of the contact problem using the general purpose finite element code ABAQUS™. Fig. 13 illustrates the comparison of results for the non-dimensional force $(P_N/\pi a^2\sigma_0)$ with the non-dimensional indentation-pre-compression stress parameter $\{G\Delta v/a\sigma_0(1-\nu)\}$ plotted in a log-scale. The general trends displayed by both sets of data show a consistent trend with some deviation between the two sets of data for values of $\log_{10}\{G\Delta v/a\sigma_0(1-\nu)\} < 0$. We also make the observation that as $\Delta v \to 0$

$$P_N = \sigma_0 \pi a^2 - \sigma_0 \pi a^2 P_N^{\sigma_0}. \tag{21}$$

In this limit, $c \equiv 1$ and from (19) we obtain $P_N^{\sigma_0} = 0.0272$. It is clear that the number of terms in the power series representation of $P_N^{\sigma_0}$ given by (19) is insufficient to render $P_N^{\sigma_0} \equiv 0$ as $c \to 1$.

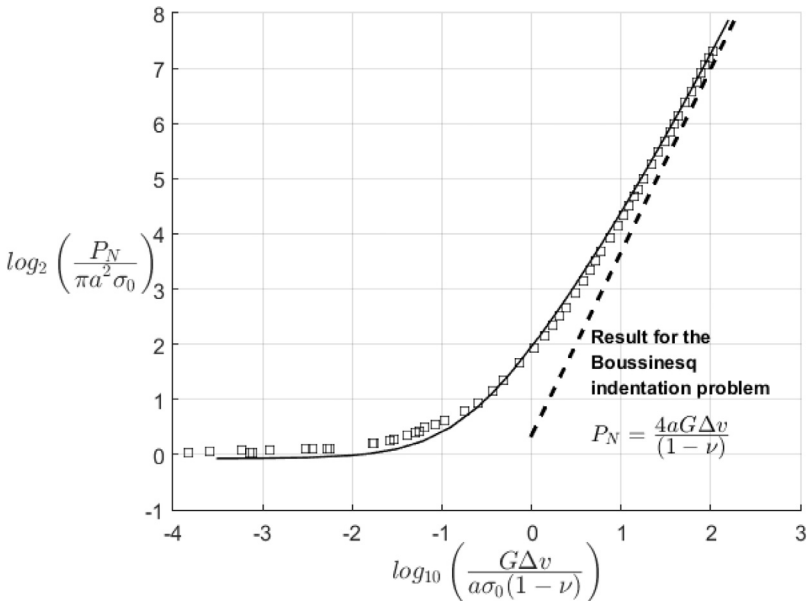

Fig. 14. The variation in the normalized force $\log_2\{P_N/\pi a^2\sigma_0\}$ generated in the indentation zone as a function of the normalized indentation-precompression parameter $\log_{10}\{G\Delta v/a\sigma_0(1-\nu)\}$. [Solid line corresponds to the analytical estimate and the squares correspond to the computational results.]

To examine the discrepancy between the analytical and computational estimates, the results are plotted on a $\log_2\{P_N/\pi a^2\sigma_0\}$ vs. $\log_{10}\{G\Delta v/a\sigma_0(1-\nu)\}$scale. The computational results are derived using both a penalty function technique and an augmented Lagrangian technique, as a constraint enforcement method, and the latter approach gives more accurate results. The range of applicability of the analytical result can be examined by specifying the values for G, σ_0, Δv, a and ν applicable to a particular problem. Consider the example where a dilatancy-induced displacement of $\Delta v \approx 0.05$ m occurs over a circular patch of $a \approx 5$ m of located at a geological interface with elasticity properties $G \approx 30$ GPa, $\nu \approx 1/3$, which is subjected to a compressive stress state of $\sigma_0 \approx 30$ MPa. For these parameters, $\log_{10}\{G\Delta v/a\sigma_0(1-\nu)\} \approx 0.85$, which indicates the applicability of the simplified analytical result, and from Fig. 12, the radius of the separation zone $b \approx 11$ m. Fig. 14 illustrates a log-log plot of the non-dimensional force $P_N/\pi a_0^2\sigma_0$ generated at the contact zone and the non-dimensional indentation displacement $G\Delta v/a\sigma_0(1-\nu)$, as obtained from the approximate analytical solution and the computational approach based on an augmented Lagrangian technique. The approximate analytical procedure and the computational scheme give very similar results and reduce to the appropriate limits as $\{G\Delta v/a\sigma_0(1-\nu)\} \in (0,\infty)$.

3. The shear behaviour of the dilatant patch

The process of shear at a dilatant zone will involve elasto-plastic processes. Ideally, the analysis of the shear rupture problem during the generation of frictional phenomena and dilatancy effects should be examined by appeal to a theory of plasticity applicable for elasto-plastic phenomena with specified failure criteria and non-associated flow rules (see e.g., Chen, 1975; Desai & Siriwardane, 1984; Davis & Selvadurai, 2003; Pietruszczak, 2010; Wan, Nicot, & Darve, 2017). In this study, we focus on the evaluation of the peak rupture that can be generated at the circular patch when dilatancy is present. To estimate the limiting response, we utilize the procedure presented by D.W. Taylor (1948) for the analysis of dilatancy processes in granular materials. (The remarkable accomplishments of D.W. Taylor in laying the foundations for important developments in the field of soil mechanics are documented in the paper by Christian and Baecher (2015)). In essence, Taylor proposes a criterion that neglects the elastic energy storage processes at the direct contact zone, when examining failure processes associated with dilatancy effects. (To a certain extent, this argument is consistent with the limit analysis concepts proposed by Drucker and Prager (1952); see also Davis & Selvadurai, 2003.) The basic hypothesis involves the relationship between the *work done by the shearing forces and normal forces* and the *energy dissipated at the frictional-dilatant region*, expressed in terms of force resultants rather than exact distributions over the contact zone. The work component W consists of the work of the shear force (P_T) acting at the onset of rupture and the work of the normal force (P_N) induced by dilatancy on the upper and lower surface: i.e.

$$W = 2P_T(\Delta u) + 2P_N(-\Delta v). \tag{22}$$

where the shear displacement Δu and the dilatancy displacement Δv are defined in Fig. 9. The energy dissipated at the dilatant circular patch is given by

$$D = 2P_N\,(\Delta u)\tan\varphi, \tag{23}$$

where φ is the contact friction angle. We note that the work of forces and dissipation on both faces of the circular patch need to be included in the formulation. In Taylor's hypothesis, the conventional relationship between Δv and Δu is through the relationship $\Delta v = \Delta u \tan\alpha_0$, where α_0 is the constant dilatancy angle.

In the current work, we extend the dilatancy concept to accommodate the following constraints: (i) the dilatancy displacement Δv should be a continuous and a symmetric function of Δu; i.e. dilatancy has attributes of a second-order effect; (ii) the dilatancy angle α can experience degradation that can be governed by a function of the relative displacement Δu, with the constraint that as the relative displacement $(\Delta u/a) \to \infty$, dilatancy effects will become negligible. The latter constraint is based on plausible physical effects of asperity degradation with increasing relative shear. In the ensuing developments, we assume that the dilatancy displacement Δv can be expressed in the form

$$\Delta v = a\left(\frac{\Delta u}{a}\right)^2 \tan\alpha, \tag{24}$$

where α is a dilatancy angle that depends on the relative shear and an arbitrary parameter that controls the intensity of the degradation of the dilatancy. Recognizing the constraints indicated earlier, we express the change in the dilatancy angle with the relative shear as follows:

$$\tan\alpha = \exp\left(-\lambda\left|\frac{\Delta u}{a}\right|\right)\tan\alpha_0, \tag{25}$$

where λ is a non-dimensional parameter and the modulus term accounts for the invariance of the degradation of the dilatancy angle on the sign of the shear displacement. From (25), we note that dilatancy can materialize only when $\Delta u/a$ is finite and dilatancy is absent when $(\Delta u/a) \to \infty$ .The validity of the proposed relationships (24) and (25) describing respectively the development of dilatancy and the deterioration of the angle of dilatancy with increasing shear needs to be verified through examination of experimental data. The Appendix A provides comparisons with available experimental data.

A number of other relationships can be postulated to accommodate the process of dilatancy degradation with increasing relative shear and a development where the degradation of the dilatancy angle is related to the plastic energy dissipation in the contact zone is presented in Appendix B. In the ensuing, however, attention is focused on estimating the enhancement of the rupture shear stress that can result from development of dilatancy at the circular patch.

Combining (22) to (25), we obtain the following relationship for the failure shear stress τ_D at a dilatant circular patch: i.e.

$$\tau_D = \sigma_0\left(1 + \frac{4G}{(1-\nu)\sigma_0\pi}\left(\frac{\Delta u}{a}\right)^2 \exp\left(-\lambda\left|\frac{\Delta u}{a}\right|\right)\tan\alpha_0 P_N^{\Delta v} - P_N^{\sigma_0}\right)\left(\tan\varphi + \frac{\Delta u}{a}\exp\left(-\lambda\left|\frac{\Delta u}{a}\right|\right)\tan\alpha_0\right), \tag{26}$$

where $P_N^{\Delta v}$ and $P_N^{\sigma_0}$ are defined by (18) and (19) respectively and the radius of the separation zone is now determined from the equation

$$\left(\frac{G}{\sigma_0(1-\nu)}\right)\left(\frac{\Delta u}{a}\right)^2 \exp\left(-\lambda\left|\frac{\Delta u}{a}\right|\right)\tan\alpha_0 c F_{\Delta v}(c) - 2F_{\sigma_0}(c) = 0 \tag{27}$$

and $F_{\Delta v}(c)$ and $F_{\sigma_0}(c)$ are defined by (10) and (15) respectively. If the contribution from $P_N^{\sigma_0}$ is neglected and as the dilatancy angle $\alpha_0 \to 0$, the result (26) reduces to the failure shear stress τ_C at a circular patch that exhibits purely Coulomb friction, $\tau_C = \sigma_0 \tan\phi$. We can define the "*Shear Stress Amplification Factor*" (*SSAF*) as

$$SSAF = \frac{\tau_D}{\tau_C} = \left(1 + \frac{4G}{(1-\nu)\sigma_0\pi}\left(\frac{\Delta u}{a}\right)^2 \exp\left(-\lambda\left|\frac{\Delta u}{a}\right|\right)\tan\alpha_0 P_N^{\Delta v} - P_N^{\sigma_0}\right)\left(1 + \frac{\Delta u}{a}\exp\left(-\lambda\left|\frac{\Delta u}{a}\right|\right)\frac{\tan\alpha_0}{\tan\varphi}\right). \tag{28}$$

4. Numerical results and concluding remarks

Since the result for the dilatancy induced shear stress amplification has been evaluated in explicit closed form, the result (28) can be evaluated quite conveniently for specific choices of the non-dimensional parameter defined by $\Gamma (= G/(1-\nu)\sigma_0)$ and the material and interface parameters ν, φ, λ and α_0. The parameter $\Gamma = 2000$ can correspond to a dilatant circular shear region in a basaltic rock at a depth of 2 km. Figs. 15 and 16 give typical results for the *Shear Stress Amplification Factor* (*SSAF*) when the initial dilatancy angle α_0 and the dilatancy angle degradation parameter λ are varied. It is clear that if the dilatancy angle does not experience a relative shear displacement-related degradation, the magnitude of the *SSAF* can increase substantially. The dilatancy angle degradation parameter also has a significant influence in attenuating the *SSAF*. Results presented in Figs. 15 and 16 are derived for two dilatancy angles of 5° and 10° respectively, which are representative of rock joints encountered under field conditions. The magnitude of the *SSAF* is clearly influenced by the initial dilatancy angle and the dilatancy degradation parameter. The exact closed form expression for the *SSAF* (28) can be conveniently evaluated, with the proviso that a numerical procedure has to be used to solve (27) for the radius of the zone of separation

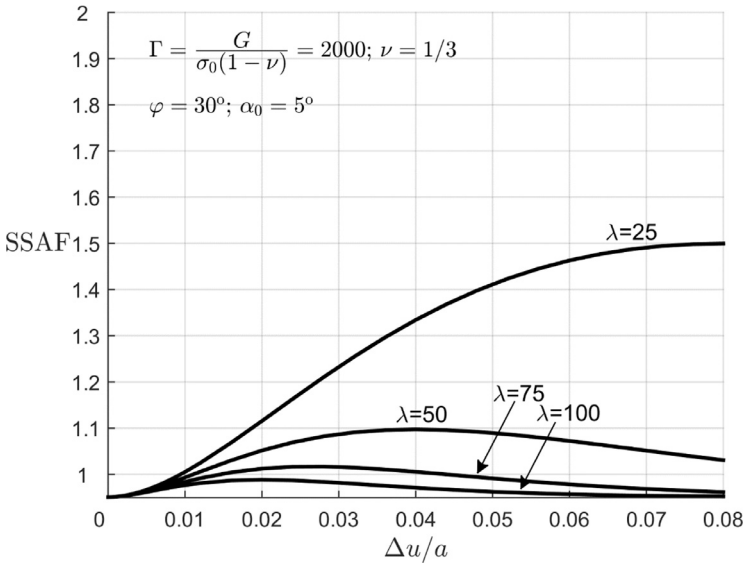

Fig. 15. Dilatancy-induced shear stress amplification at a circular patch. Initial dilatancy angle is 5°.

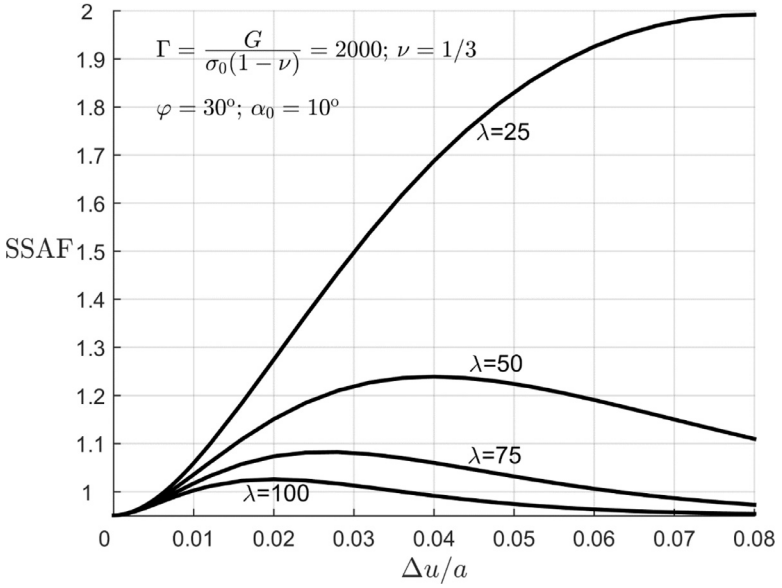

Fig. 16. Dilatancy-induced shear stress amplification at a circular patch. Initial dilatancy angle is 10°.

b. It should be noted that the limiting value of *SSAF* in Figs. 15 and 16 is not exactly equal to 1, which is caused by the errors in the expressions for F_{σ_0}, $F_{\Delta\nu}$, $P_N^{\sigma_0}$, $P_N^{\Delta\nu}$ as the ratio $c = a/b \to 1$.

It is of interest to obtain a simplified expression for *SSAF* which is valid for small dilatancy-induced displacement $\Delta\nu$. When $\Delta\nu \to 0$ it follows that $\Delta u \to 0$ and from (27), $F_{\sigma_0}(c) \to 0$. Thus, the ratio $c \to 1$ as the root of the equation $F_{\sigma_0}(c) = 0$ is $c = 1.0761 \approx 1$. When c is close to unity, $P_N^{\sigma_0} \to 0$ and $P_N^{\Delta\nu} = 2.727$. Hence, from (28) we can write the estimate for *SSAF* valid for small values of $\Delta\nu/a$

$$SSAF \approx \frac{\tau_D}{\tau_C} = \left(1 + 2.727\frac{4G}{(1-\nu)\sigma_0\pi}\left(\frac{\Delta u}{a}\right)^2 \exp\left(-\lambda\left|\frac{\Delta u}{a}\right|\right)\tan\alpha_0\right)\left(1 + \frac{\Delta u}{a}\exp\left(-\lambda\left|\frac{\Delta u}{a}\right|\right)\frac{\tan\alpha_0}{\tan\varphi}\right) \tag{29}$$

Figs. 17 and 18 present the results for the *SSAF* determined using the simplified expression (29).

To present these numerical results in a practical context, it is instructive to obtain estimates of the typical values for relative shear that can materialize on contact regions of natural fractures ($\Delta u/a$). The results shown in Fig. 19 were obtained from the data presented by Nadeau and Johnson (1998) in their studies related to the earthquake in Parkfield, CA.

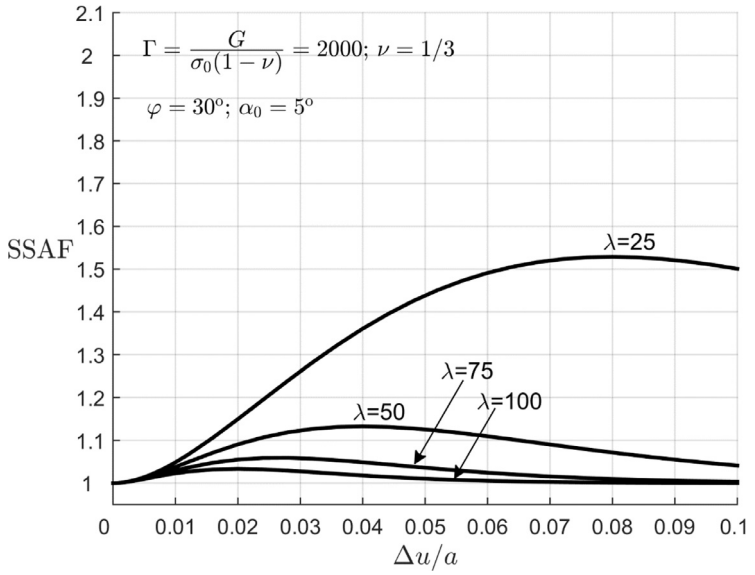

Fig. 17. Approximate estimate for the dilatancy-induced shear stress amplification at a circular patch using the result (29) and for an initial dilatancy angle of 5°.

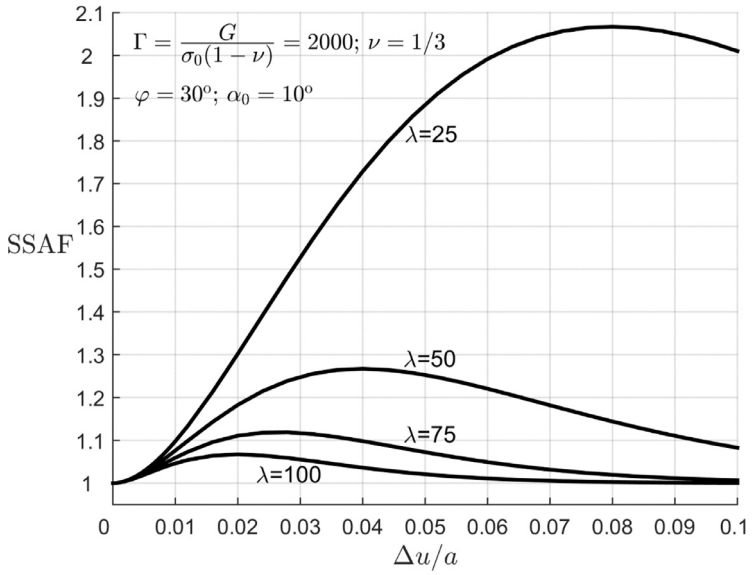

Fig. 18. Approximate estimate for the dilatancy-induced shear stress amplification at a circular patch using the result (29) and for an initial dilatancy angle of 10°.

The data indicates the range of values of the relative shear associated with the event and in particular the larger event numbers that materialize at low values of $(\Delta u/a)$, which corresponds to the range of relative displacements that are most likely to contribute to dilatancy phenomena. Fig. 19 also shows the stress drop (see Eq. 27 of Nadeau and Johnson (1998) and also Eshelby (1957)) as a function of the relative shear at the contact region. The values presented by Nadeau and Johnson (1998) appear to be $\sim$ 2- to 3 orders of magnitude higher than typical values that range from $\sim$ 1 to 10 MPa (Hanks, 1977; Allmann & Shearer, 2009) and are associated with earthquakes that exhibited higher ratios of relative slip. Sammis, Nadeau, and Johnson (1999) noted that these high values of stress drop may be explained by a fractal spatial distribution of smaller (stronger) asperities along a larger (weaker) asperity leading to a rescaling factor of 20. Their model does not account for dilatancy-induced shear behavior that would additionally scale the results as is shown in our relatively rudimentary dilatant-asperity model.

In Fig. 20 we examine the effect of the dilatant asperity on the individual stress drops calculated by Nadeau and Johnson (1998). Nadeau and Johnson (1998) used Eshelby's (1957) calculation of a thin penny-shaped crack embedded in a homogeneous elastic infinite space to relate the amount of average shear stress $(\Delta\sigma)$ needed to 'slip' (Δu) at the cracks

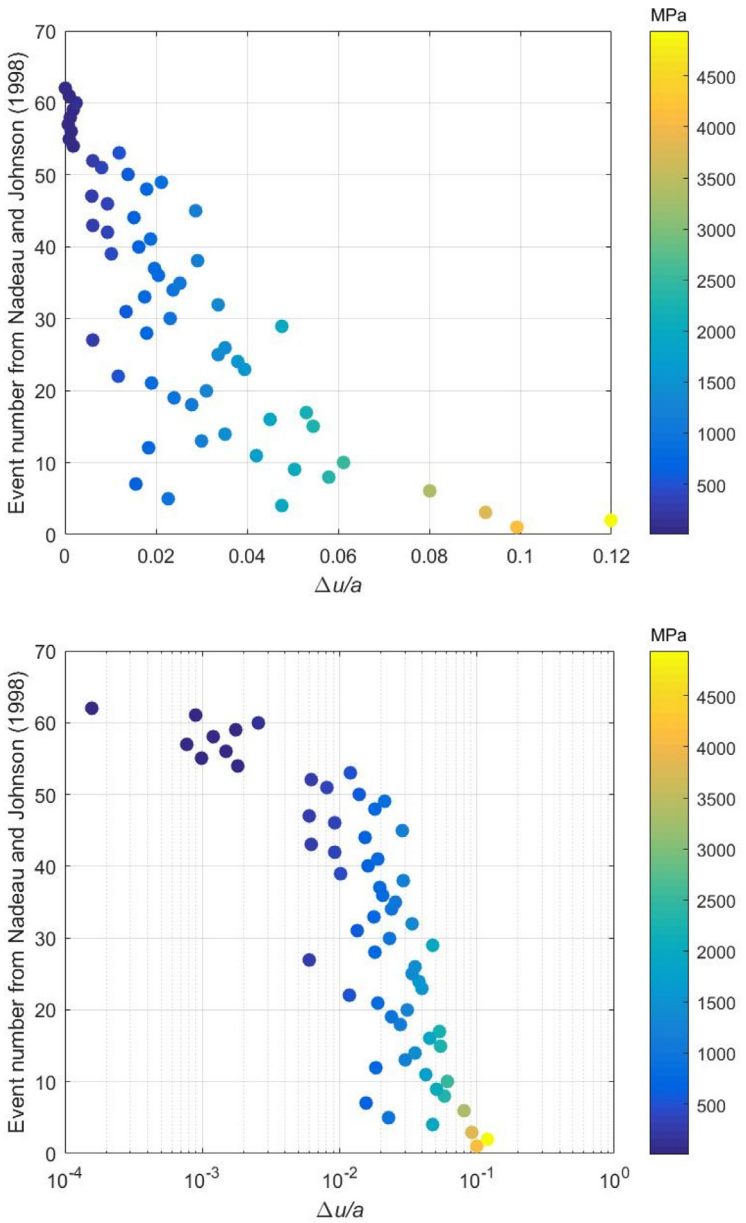

Fig. 19. Variation of event number for the Parkfield earthquake as a function of the relative shear at the contact region. For clarity, the upper figure has a linear representation of the relative slip and the lower figure is identical but with a logarithmic representation of the relative slip.

surfaces via the elastic parameters G and ν. As determined by Eshelby (1957) and assuming a Poisson's ratio $\nu = 0.3$, this relationship can be written as

$$\Delta\sigma = \frac{7\pi}{16} G\left(\frac{\Delta u}{a}\right). \tag{30}$$

In this basic interpretation, only shear motion occurs on the crack and the term 'stress drop' refers to the shear stress required to initiate deformations at the surfaces of the crack. We see that this expression has relative slip $(\Delta u/a)$ making it easily compatible with our derivation of the *SSAF* shown in Eq. (28) and in Figs. 15 to 16. The gray line in Fig. 20 represents a scaling factor of 1, implying that the amplification of shear stress is uninfluenced by dilatancy. The stress drops from events detailed by Nadeau and Johnson (1998) are shown as black dots and a corrected value of stress drop using Eq. (29) is shown for various levels of the dilatancy angle degradation parameter $\lambda = 25$, 50, 75 and 100, in a clockwise manner from top-left. Stress drop correction was performed by dividing the Eshelby stress drop $(\Delta\sigma)$ by the shear stress amplification factor *SSAF* (Eq. (29)) which varied with the relative slip $(\Delta u/a)$ for the individual events. This is justified if we consider that

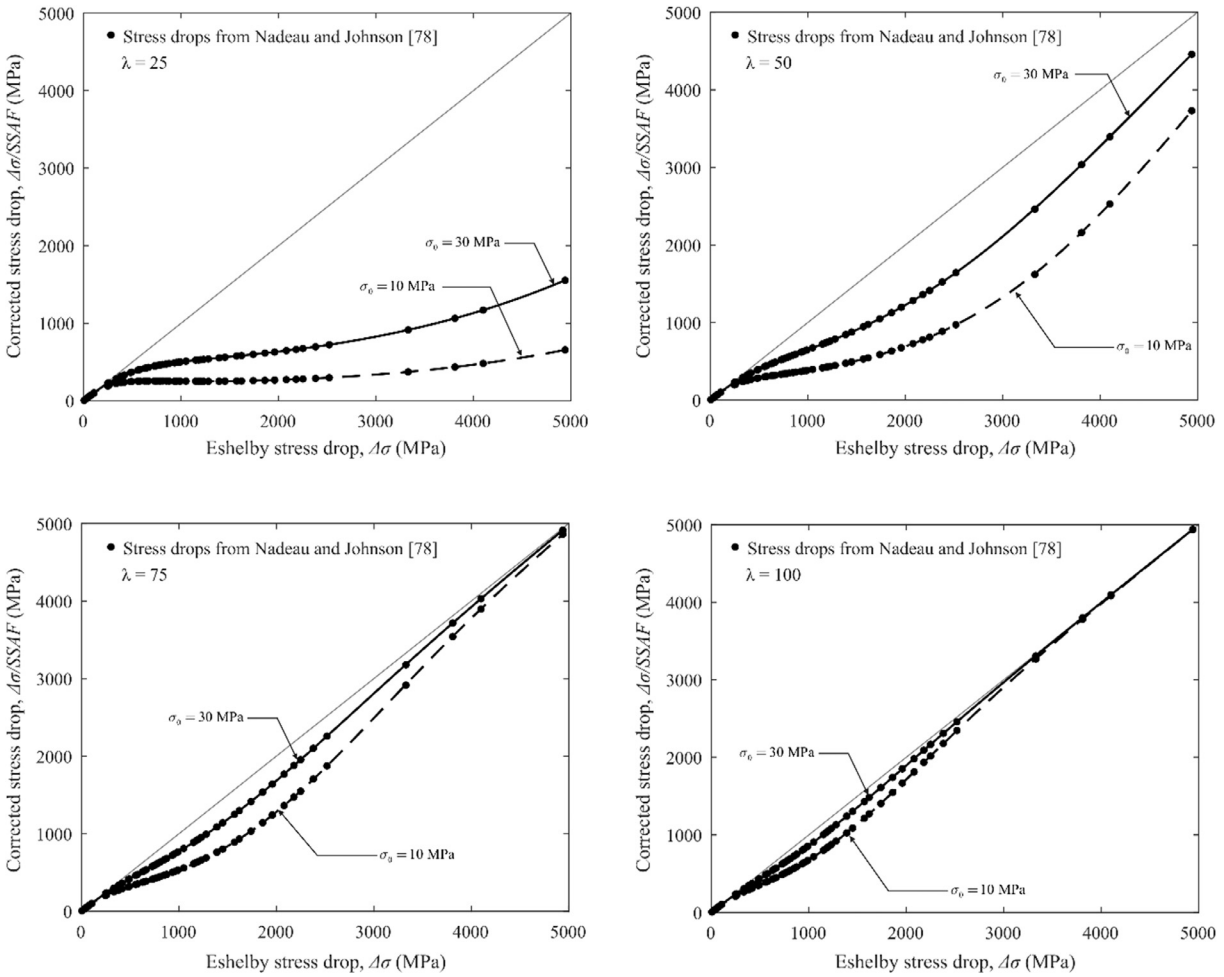

Fig. 20. The stress drops from events catalogued in Fig. 19 are shown as black dots and a corrected value of stress drop was done using equation (29) for various levels of the dilatancy angle degradation parameter $\lambda = 25$, 50, 75 and 100 (clockwise from top-left). Stress drop correction was performed by dividing the Eshelby stress drop by the shear stress amplification factor (Eq. (29)) which varied with the relative slip ($\Delta u/a$) for the individual events.

the earthquakes occurred on a preexisting fault and exhibited the same simple Coulomb friction that reduced to a failure shear stress $\tau_C = \sigma_0 \tan\varphi$ in the same way as the dilatant asperity. We can then examine the corrected stress drop $\Delta\sigma_c$ as

$$\Delta\sigma_c = \frac{C \cdot G(\Delta u/a)}{SSAF}, \tag{31}$$

where $C = 7\pi/16$ for $\nu = 0.3$ and the *SSAF* is given in (28) and (29). Fig. 20 shows the corrected stress drop where each model used was given elastic properties $G = 30$ MPa and $\nu = 0.3$, and interface parameters $\varphi = 30^o$ and $\alpha_0 = 10^o$ and the effect of the normal stress was examined for two-levels of compressive normal stress: $\sigma_0 = 30$ MPa (solid line) and $\sigma_0 = 10$ MPa (dashed line). We note that for low $\lambda = 25$, the stress drop correction factor may be as high as 8.9 and 3.6 at the lower and higher compressive stresses, respectively. It should be noted that a decrease in compressive stress could dramatically influence the dilatant asperity behavior in terms of the *SSAF* calculated in (29). Effective normal stress (see Scholz, 1998) is determined by considering the lithostatic load reduced by the pore pressure and is analogous to compressive stress σ_0 in this model. Local variations in effective normal stress has been suggested in a wide range of geological settings (Bilek & Lay, 1999; Kodaira et al., 2004; Kitajima & Saffer, 2012) and may be due to a variety of reasons, such as, local permeability enhancement via fault valves (see Sibson, 1992) leading to a change in pore fluid pressure, the topographic interaction of the faulting surface where strong asperities and incompetent gouge (matrix) are present, local variations in material properties (Rice & Cocco, 2007), pore pressure coupled poroelastic effects (Cocco & Rice, 2002; Selvadurai, Suvorov, & Selvadurai, 2015; Selvadurai & Suvorov, 2016), among others. Low effective normal stresses and its influence on frictional behaviors have been successfully modelled in numerical studies (e.g., Segall & Liu, 2015; Luo & Ampuero, 2018) and also in the laboratory (Linker & Dieterich, 1992; Marone, 1998; Hong & Marone, 2005; Scuderi & Colletini, 2016; Scuderi, Collettini, & Marone, 2017). We can conclude that when the ratio of relative slip increases the assumptions implicit in the effective stress drop model (see

Eq. (30) and also Brune (1970, 1971) and Eshelby (1957)) do not apply due to differences in the boundary value problem associated with the modelling. The relatively large stress drops noted by Nadeau and Johnson (1998), up to 4500 MPa stress drops for the smallest events, are in contradiction with estimates obtained for small Parkfield earthquakes for which stress drops of the order of 1-10 MPa (Imanishi et al., 2004). High stress drop hypothesis results from the assumption that slip occurring on asperities is uniquely due to purely in-plane slip without no interface dilation. A currently accepted explanation is that through the earthquake nucleation model, for which aseismic slip is found to play an important role, a proportion of slip is released aseismically and is found to depend on the asperity size (Chen and Lapusta, 2009). While this model is important, we show that the dilation-induced SSAF could also be a mechanism that would result in an amplification of the Eshelby stress drop. Future investigations should focus on the characterization of the dilatancy angle degradation parameter λ, which the authors believe could be accomplished in a laboratory setting. More intricate degradation laws may provide more realistic results than the model detailed in this study and indicated by the Eq. (25).

Acknowledgements

The authors are grateful to the Editor, Professor Mark Kachanov for highly constructive comments, which led to improvements in the presentation. The work described in the paper was supported by a Discovery Grant awarded by the Natural Sciences and Engineering Research Council of Canada. The view of the "*Balancing Rock*" in Namibia, shown in Figure 2 is attributed to Getty Images http://www.gettyimages.ca/detail/dv424076?Language=en-US. The first author would like to expresses his thanks to Mr. Peter Pohl-Sitzler of Pohl-Sitzler Lawyers of Freiburg, for arranging the visit to Herrenknecht AG, Schwanau, Baden-Wurtemburg. A special thanks for Mr. Josef Gruseck of the Herrenknecht Management Team for conducting a site visit of the TBM manufacturing facilities at Schwanau.

Appendix A

In Taylor's model, the development of dilatancy at the interface is *uninfluenced* by either the normal stress acting on the contact zone and/or the local normal stiffness. This would suggest that a constant dilatancy angle is appropriate for fractures located at *shallow depths* where the normal stresses have no appreciable influence on the dilatant displacements that can be induced under shear. In the case of fractures that are *deeply located*, the normal stresses and the local elasticity at the contact zone can influence the development of dilatancy and, if shear deformations are enforced, the end result will be the alteration of the dilatancy angle through the development of asperity breakage and gouge generation. Ideally, the development of dilatancy at a geological interface should take into account several factors, including the normal stress state, the asperity profile and its scale, the elasticity and the failure characteristics of the rock material composing the interface. Such an all-encompassing treatment will be useful but requires extensive experimental work. The experimental investigations conducted by various researchers have been summarized in Bandis, Lumsden, and Barton (1981), Plesha (1987), Nguyen and Selvadurai (1998), Morris (2003), Barton (2013) and Prasseyto, Guttierrez, and Barton (2017). In terms of potential applications to deep earth settings, where scale effects can be important, the experiments conducted by Bandis et al. (1981) and Olssen and Barton (2001) can be used to illustrate the alterations in the dilatancy. There are no preferences for selecting these studies except that the results by Bandis et al. (1981) are from tests performed on a large natural fracture of length (30 cm) in a weathered granite with an initial dilatancy angle α_0 of approximately 7.8° and the results by Olssen and Barton (2001) conducted on granitic rocks from the Åspö Hard Rock Laboratory (HRL) in Sweden account for variations in the normal stiffness and an initial dilatancy angle of approximately 11.3°. Since the experimental data given by Bandis et al. (1981) and Olssen and Barton (2001) are presented as absolute values of Δu (in mm) and Δv (in mm), in order to examine the trends that can be associated with predictions of the dilatancy relationships proposed by (24) and (25), we modify these equations to the form

$$\Delta v = C_S(\Delta u)^2 \tan\alpha \tag{A1}$$

where C_S is an arbitrary constant with units mm^{-1}. Similarly, the variation in the dilatancy angle is specified by

$$\tan\alpha = \exp\left(-\lambda_S|\Delta u|\right)\tan\alpha_0 \tag{A2}$$

where λ_S is an arbitrary constant with units mm^{-1}. For purposes of comparison, we also consider Taylor's linear relationship between Δu and Δv modified to account for alterations to the dilatancy angle with shear deformation; i.e.

$$\Delta v = C_T(\Delta u)\tan\alpha \tag{A3}$$

where C_T is a non-dimensional arbitrary constant. The variation in the dilatancy angle is specified by

$$\tan\alpha = \exp\left(-\lambda_T|\Delta u|\right)\tan\alpha_0 \tag{A4}$$

and λ_T is an arbitrary constant with units mm^{-1}. The dilatancy relationships (A1) to (A4) are indeterminate to within the arbitrary constants C_S, λ_S, C_T and λ_T. They can be assigned specific values by considering an appropriate curve fitting procedure to yield a minimum error between the theoretical predictions and the experimental data. Since we are interested in observing the general trends, in the ensuing we select values of these parameters that will approximately match the trends in the experimental data. We further note that the parameters λ_S and λ_T control the shape of the curve of

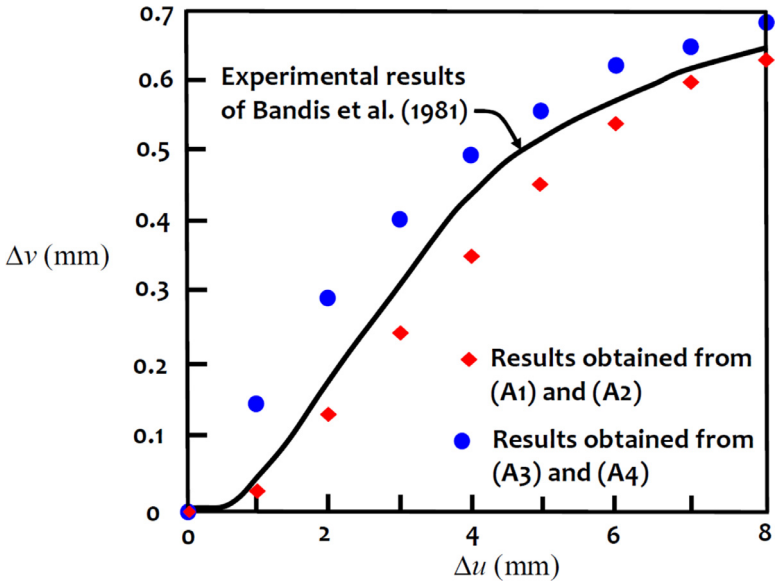

Fig. A.1. The variation in the dilatancy displacement with relative shear. The solid line corresponds to the experimental data obtained from Bandis et al. (1981). The red diamonds correspond to the data obtained from the quadratic relationship proposed in this study. The blue circles correspond to the results obtained from the linear Taylor relationship modified to account for degradation of the dilatancy angle with relative shear displacement. (For interpretation of the references to colour in this figure legend, the reader is referred to the web version of this article.)

Δu vs. Δv and for large values of these parameters, the curves can display a reduction in the dilatancy displacement Δv with increasing relative shear, which is not evident in the experimental data. The relevant experimental result obtained by Bandis et al. (1981) for the variation in the dilatancy displacement Δv with shear displacement Δu is shown in Fig. A1. Typical results obtained from the model proposed in the current study and defined by the relationships (A1) and (A2) are also shown in Fig. A1 as diamonds and the parameter estimates are given by

$$C_S \approx 0.36 \text{ mm}^{-1}; \qquad \lambda_S \approx 0.20 \text{ mm}^{-1} \tag{A5}$$

The direct correlation between the values of λ used in Figs. 15–18 and the value of λ_S given in (A5) is not feasible although $\lambda = a\lambda_S$. As an approximation, considering the length of the fracture ($2a \approx 400$ mm) used in the tests conducted by Bandis et al. (1981), the value of $\lambda \approx 40$ is in the same range for the numerical results presented in Figs. 15–18. Typical results obtained from the modified Taylor model defined by the relationships (A3) and (A4) are also shown in Fig. A1 as solid circles and the parameter estimates are given by

$$C_T \approx 1.3 \qquad \lambda_T \approx 0.09 \text{ mm}^{-1} \tag{A6}$$

The results clearly demonstrate that the relationships proposed in this study, which account for the exponential variation in the dilatancy angle with progressive shear displacement Δu, is able to replicate the experimental trends reasonably well. Furthermore, the experimental data are bounded by the relationships that are based on the quadratic relationship proposed in this study and the Taylor's linear relationship modified to account for degradation of the dilatancy angle with increasing shear displacement Δu.

We next consider the results presented by Olssen and Barton (2001) for the variation in the dilatancy displacement Δv with relative shear Δu. To keep the comparisons to a minimum we focus attention on the experimental results obtained for the case involving the largest normal stiffness, as shown in Fig. A2. For this particular case, the initial dilatancy angle α_0 is approximately 11.3°. Typical results obtained from the model proposed in the current study and defined by the relationships (24) and (25) are also shown in Fig. A2 in a diamond notation and the parameter estimates are given by

$$C_S \approx 0.13 \text{ mm}^{-1}; \qquad \lambda_S \approx 0.10 \text{ mm}^{-1} \tag{A7}$$

Typical results obtained from the modified Taylor model defined by the relationships (A3) and (A4) are also shown in Fig. A2 as solid circles and the parameter estimates are given by

$$C_T \approx 1.0 \qquad \lambda_T \approx 0.05 \text{ mm}^{-1} \tag{A8}$$

The theoretical estimates are governed by the parameters sets (C_S, λ_S) and (C_T, λ_T), which can be adjusted to conform to the experimental data. The purpose of the comparisons with experimental data does not constitute a prediction, rather the intention is to demonstrate that the form of the proposed theoretical relationships (24) and (25) provide trends for the dilatancy development that is consistent with experimental observations. In an actual application to a practical situation, appropriate experimental data will be needed to develop a consistent dilatancy relationship.

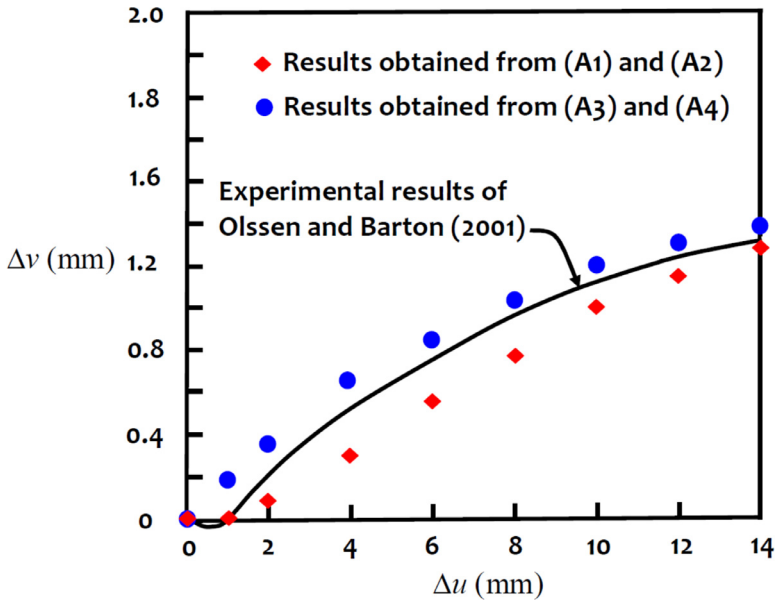

Fig. A.2. The variation in the dilatancy displacement with relative shear. The solid line corresponds to the experimental data obtained from Olssen and Barton (2001). The red diamonds correspond to the data obtained from the quadratic relationship proposed in this study. The blue circles correspond to the results obtained from the linear Taylor relationship modified to account for degradation of the dilatancy angle with relative shear displacement. (For interpretation of the references to colour in this figure legend, the reader is referred to the web version of this article.)

Appendix B

The change in the dilatancy angle α, as depicted by (25), does not account for any physical phenomenon contributing to the degradation process. An alternative development for the alteration in the dilatancy angle can relate the variation in the dilatancy angle to the frictional energy dissipation at the dilatant circular patch (Selvadurai & Nguyen, 1999). The term $(P_N/\sigma_0\pi a^2)(\Delta u/a)\tan\varphi$ is a measure of the frictional energy dissipation and the parameter λ introduced in (25) can be varied to account for the intensity of the micromechanical degradation processes at the contacting surfaces. Using the expression for $(P_N/\sigma_0\pi a^2)$ given by (17), the dilatancy-induced axial displacement of the circular patch, where the dilatancy process is defined by (24) and the degradation of dilatancy angle is defined by (25), the equivalent expression for energy dissipation D can be expressed in the form

$$D = 2P_N\,(\Delta u)\tan\varphi = 2\sigma_0\pi a^2\,(\Delta u)\left(1+\frac{4G}{\pi(1-\nu)\sigma_0}\left\{\frac{\Delta v}{a}\right\}P_N^{\Delta v}-P_N^{\sigma_0}\right)\tan\varphi \tag{B1}$$

where

$$\frac{\Delta v}{a} = \left(\frac{\Delta u}{a}\right)^2 \tan\left(\alpha_0 \exp\left\{-\frac{\lambda P_N}{\sigma_0\pi a^2}\left|\frac{\Delta u}{a}\right|\tan\varphi\right\}\right) \tag{B2}$$

From (B1) and (B2) it is evident that when interface degradation is taken into consideration, the energy dissipation is a highly non-linear function of the dilatancy displacement Δv. Some progress can be made by substituting (17) in (B2) and developing a series expansion for $\Delta v/a$ in terms of $(\Delta u/a)$. We can show that

$$\frac{\Delta v}{a} = \left(\frac{\Delta u}{a}\right)^2 \tan\left(\alpha_0\exp\{-\Omega\}\right) - \frac{4G\lambda\tan\varphi}{\pi(1-\nu)\sigma_0}\left(\frac{\Delta u}{a}\right)^3\left\{\sec^2(-\Omega)\right\}P_N^{\Delta v}\alpha_0\left(\frac{\Delta v}{a}\right) \tag{B3}$$

where

$$\Omega = \lambda\left(\frac{\Delta u}{a}\right)\left(1-P_N^{\sigma_0}\right)\tan\varphi \tag{B4}$$

If in (B3) terms of order higher than $(\Delta u/a)^2$ are neglected and the truncation error term $P_N^{\sigma_0}$ is set to zero, then a simplified expression for $(\Delta v/a)$ can be written in the form

$$\frac{\Delta v}{a} \approx \left(\frac{\Delta u}{a}\right)^2 \tan\left(\alpha_0 \exp\left\{-\lambda\left|\frac{\Delta u}{a}\right|\tan\varphi\right\}\right) \tag{B5}$$

In addition, the expression (17) can be re-written as

$$\frac{P_N}{\sigma_0 \pi a^2} = 1 + \frac{4G}{(1-\nu)\sigma_0 \pi}\left\{\left(\frac{\Delta u}{a}\right)^2 \tan\left(\alpha_0 \exp\left\{-\lambda\left|\frac{\Delta u}{a}\right| \tan\varphi\right\}\right)\right\} P_N^{\Delta\nu} \tag{B6}$$

Considering (22) and (26), the average rupture stress at the dilatant interface can be written as

$$\begin{aligned}\tau_D = &\left[1 + \frac{4G}{(1-\nu)\sigma_0 \pi}\left(\frac{\Delta u}{a}\right)^2 \tan\left(\alpha_0 \exp\left\{-\frac{\lambda P_N}{\sigma_0 \pi a^2}\left|\frac{\Delta u}{a}\right| \tan\varphi\right\}\right) P_N^{\Delta\nu} - P_N^{\sigma_0}\right] \\ &\times\left\{\tan\varphi + \left(\frac{\Delta u}{a}\right)\tan\left(\alpha_0 \exp\left\{-\frac{\lambda P_N}{\sigma_0 \pi a^2}\left|\frac{\Delta u}{a}\right| \tan\varphi\right\}\right)\right\}\end{aligned} \tag{B7}$$

It is also convenient to consider rupture stress (B7) for a *dilatant circular patch*, which can be normalized with respect to the corresponding value for the *non-dilatant circular patch exhibiting only Coulomb friction* (τ_C). Assuming that $P_N^{\sigma_0} \approx 0$, the *Shear-Stress-Amplification-Factor* (*SSAF*) can now be defined as

$$SSAF = \frac{\tau_D}{\tau_C} = \left[1 + \frac{4G}{(1-\nu)\sigma_0\pi}\left(\frac{\Delta u}{a}\right)^2 \tan\left(\alpha_0 \exp\left\{-\frac{\lambda P_N}{\sigma_0 \pi a^2}\left|\frac{\Delta u}{a}\right| \tan\varphi\right\}\right) P_N^{\Delta\nu}\right] \times\left\{1 + \frac{1}{\tan\varphi}\left(\frac{\Delta u}{a}\right)\tan\left(\alpha_0 \exp\left\{-\frac{\lambda P_N}{\sigma_0\pi a^2}\left|\frac{\Delta u}{a}\right| \tan\varphi\right\}\right)\right\} \tag{B8}$$

where the expression for $P_N/\sigma_0\pi a^2$ is now given by (B6) and the radius of the zone of separation required to calculate $P_N^{\Delta\nu}$ is determined by (27).

Limiting Cases

(i) As is evident from (B8), as $\alpha_0 \to 0$ (i.e. no dilatant phenomena) we obtain $SSAF \to 1$ with the assumption that $P_N^{\sigma_0} \approx 0$.
(ii) As $\lambda \to 0$, from (25) we note that when the degradation of dilatancy is suppressed, i.e. $\alpha = \alpha_0$, (B8) gives

$$SSAF = \left[1 + \frac{4G}{(1-\nu)\sigma_0\pi}\left(\frac{\Delta u}{a}\right)^2 P_N^{\Delta\nu}\tan\alpha_0\right]\left\{1 + \frac{1}{\tan\varphi}\left|\frac{\Delta u}{a}\right|\tan\alpha_0\right\} \tag{B9}$$

and when the relative movement is suppressed, i.e. $(\Delta u/a) \to 0$, the effects of dilatancy are suppressed and $SSAF \to 1$.

References

Aleynikov, S. M. (2011). *Spatial contact problems in geotechnics: Boundary element method*. Berlin: Springer-Verlag.
Aliabadi, M., & Brebbia, C. A. (1993). *Computational methods in contact mechanics*. Southampton: Computational Mech Publ.
Allman, B. P., & Shearer, P. M. (2009). Global variations of stress drop for moderate to large earthquakes. *Journal of Geophysical Research, Vol. 114*, B01310.
Anoosheshpoor, A., & Brune, J. N. (2001). Quasi-static slip-rate shielding and creeping zones as an explanation for small repeating earthquakes at Parkfield. *Bulletin of the Seismological Society of America, Vol. 91*, 401–403.
Archard, J. F. (1953). Contact and rubbing of flat surfaces. *Journal of Applied Physics, Vol. 24*, 981–988.
Bandis, S. C., Lumsden, A. C., & Barton, N. R. (1981). Experimental studies of scale effects on the shear behaviour of joints. *International Journal of Rock Mechanics and Mining Sciences, Vol. 18*, 1–21.
Barber, J. R. (2018). *Contact mechanics*. Berlin: Springer-Verlag.
Barton, N. R. (2013). Shear strength criteria for rock, rock joints, rockfill and rock masses: Problems and some solutions. *Journal of Rock Mechanics and Geotechnical Engineering, Vol. 5*, 249–261.
Barton, N. R., & Choubey, V. (1977). The shear strength of rock joints in theory and practice. *Rock Mech, Vol. 10*, 1–54.
Barton, N. R, & Stephansson, O. (Eds.) (1990). *Rock joints*. In *Proceedings of the International Symposium on Rock Joints*. Loen, Norway: AA Balkema, Rotterdam.
Beeler, N. M., Lockner, D. A., & Hickman, S. H. (2001). A simple stick-slip and creep-slip model for repeating earthquakes and implication for microearthquakes at Parkfield. *Bulletin of the Seismological Society of America, Vol. 91*, 1797–1804.
Ben-Zion, Y., & Sammis, C. (Eds.). (2010). *Mechanics, structure and evolution of fault zones*. Vienna: Birkhauser Geoscience.
Bilek, S. L., & Lay, T. (1999). Rigidity variations with depth along interpolate megathrust faults in subduction zones. *Nature, Vol. 400*, 443–446.
Borucki, L. J. (2002). Mathematical modelling of polish-rate decay in chemical-mechanical polishing. *Journal of Engineerng Mathematics, Vol. 43*, 105–114.
Borucki, L. J., Witelski, T., Please, C., Kramer, P., & Schwendeman, D. (2004). A theory for pad conditioning for chemo-mechanical polishing. *Journal of Engineerng Mathematics, Vol. 50*, 1–24.
Boussinesq, J. (1885). *Application des Potentiels a L'etude de l'equilibre et due Mouvement des Solides Elastique*. Paris: Gauthier Villars.
Bowden, F. P., & Tabor, D. (1986). *Friction and lubrication of solids*. Oxford: Clarendon Press.
Brace, W. F., & Martin, R. J. (1968). The test law for effective stress for crystalline rocks of low porosity. *International Journal of Rock Mechanics and Mining Science, Vol. 5*, 415–436.
Broberg, B. K. (1999). *Cracks and fracture*. San Diego: Academic Press.
Brune, J. N. (1970). Tectonic stress and the spectra of seismic shear waves from earthquakes. *Journal of Geophysical Research, Vol. 75*, 4997–5009.
Brune, J. N. (1971). Correction to "Tectonic stress and the spectra of seismic shear waves from earthquakes". *Journal of Geophysical Research, Vol. 76*, 5002.
Chen, W.-F. (1975). *Limit analysis and soil plasticity, developments in geotechnical engineering*: Vol. 7. Amsterdam: Elsevier.
Chen, T., & Lapusta, N. (2009). Scaling of small repeating earthquakes explained by interaction of seismic and aseismic slip in a rate and state fault model. *Journal of Geophysical Research, Vol. 114*, B01311. doi:10.1029/2008JB005749.
Chen, Y., & Sammis, C. G. (2003). Asperity models for earthquakes. *Bulletin of the Seismological Society of America, Vol. 94*, 1792–1802.
Cherepanov, G. P. (1979). *Mechanics of brittle fracture*. New York: McGraw-Hill (Translation edited by R. De Wit, A.C. Cooley and A.L. Peabody).
Christian, J. T., & Baecher, G. P. (2015). D.W. Taylor and the foundations of modern soil mechanics. *Journal of Geotechnical and Geoenvironmental Engineering, Vol. 141*, 02514001.
Ciavarella, M. (2016). On the effect of wear on asperity height distributions, and the corresponding effect in the mechanical response. *Tribology International, Vol. 101*, 164–167.
Cocco, M., & Rice, J. R. (2002). Pore pressure and poroelasticity effects in Coulomb stress analysis of earthquake interactions. *Journal of Geophysical Research, Vol. 107* (B2). doi:10.1029/2000JB000138.
Cooke, J. C. (1963). Some further triple integral equation solutions. In *Proceedings of the Edinburgh Mathematical Society: Vol. 13* (pp. 303–316).
Curnier, A. (Ed.). (1992). *Contact mechanics international symposium*. EPFL, Lausanne: Laboratoire Mecanique Appliquee.
Davis, R. O., & Selvadurai, A. P. S. (1996). *Elasticity and geomechanics*. Cambridge: Cambridge University Press.
Davis, R. O., & Selvadurai, A. P. S. (2003). *Plasticity and geomechanics*. Cambridge: Cambridge University Press.
de Pater, A. D., & Kalker, J. J. (1975). The mechanics of contact between deformable bodies. Proc IUTAM Symposium, *Ensched*. The Netherlands: Delft University Press.
Desai, C. S., & Christian, J. T. (Eds.). (1975). *Numerical Methods in Geotechnical Engineering*. New York: McGraw-Hill.
Desai, C. S., & Ma, Y. (1992). Modelling of joints and interfaces using the disturbed-state concept. *International Journal for Numerical and Analytical Methods in Geomechanics, Vol. 16*, 623–653.
Desai, C. S., & Siriwardane, H. J. (1984). *Constitutive laws for engineering materials: With emphasis on geologic materials*. Englewood Cliffs, NJ: Prentice-Hall.
Drucker, D. C., & Prager, W. (1952). Soil mechanics and plastic analysis or limit design. *Quarterly of Applied Mathematics, Vol. 10*, 157–165.
Duvaut, G., & Lions, J. L. (1976). *Inequalities in mechanics and physics. A series of comprehensive studies in mathematics*. Heidelberg: Springer-Verlag.

Eshelby, J. D. (1957). The determination of the elastic field of an ellipsoidal inclusion and related problems. In *Proceedings of the Royal Society, Series A: Vol. 241* (pp. 376–396).
Fichera, G. (1972). Boundary value problems of elasticity with unilateral constraints. In C. Truesdell (Ed.), *Handbuch der Physik, Mechanics of Solids II* (pp. 391–424). Berlin: Springer-Verlag. vol. VIa/2.
Frank, F. C. (1965). On dilatancy in relation to seismic sources. *Reviews in Geophysics and Space Physics, Vol. 3*, 485–503.
Galin, L. A. (1961). *Contact problems in the theory of elasticity*. Raleigh NC: North Carolina State College (Translated from Russian by H. Moss).
Gens, A. (1995). In A. P. S. Selvadurai, & M. J. Boulon (Eds.), *Mechanics of geomaterial interfaces* (pp. 395–420). New York: Elsevier.
Gladwell, G. M. L. (1980). *Contact problems in the classical theory of elasticity*. The Netherlands: Sijthoff and Nordhoff, Alphen aan den Rijn.
Gladwell, G. M. L. (1995). On contact problems for a medium with rigid flat inclusions of arbitrary shape. *International Journal of Solids and Structures, Vol. 32*, 383–389.
Gladwell, G. M. L., & Hara, T. (1981). The contact problem for a rigid obstacle pressed between two dissimilar halfspaces. *Quarterly Journal of Mechanics and Applied Mathematics, Vol. 34*, 251–263.
Goldberg, R., Siman-Tov, S., & Emmanuel, S. (2016). Weathering resistance of carbonate fault mirrors promotes rupture localization. *Geophysical Research Letters, Vol. 43*, 3105–3111.
Goodman, R. E., & Dubois, J. (1972). Duplication of dilatancy in analysis of jointed rocks. *Journal of the Soil Mechanics and Foundations Division, Proceedings of the ASCE, Vol. 98*, 399–422.
Gudehus, G. (1977). *Finite elements in geomechanics*. London: John Wiley.
Hanks, T. C. (1977). Earthquake stress drops, ambient tectonic stresses and stresses that drive plate motions. *Pure and Applied Geophysics, Vol. 115*, 441–458.
Harding, J. W., & Sneddon, I. (1945). The elastic stresses produced by the indentation of the plane of a semi-infinite elastic solid by a rigid punch. *Proceedings of the Cambridge Philosophical Society, Vol. 41*, 16–26.
Hisano, M. (2018). *Friction at the atomic level-atomistic approaches in tribology*. Weinheim, Germany: Wiley-VCH.
Hong, T., & Marone, C. (2005). Effects of normal stress perturbations on the frictional properties of simulated faults. *Geochemistry, Geophysics, Geosystems, Vol. 6*, 1–19 Q03012. doi:10.1029/2004GC000821.
Imanishi, K., Ellsworth, W. L., & Prejean, S. G. (2004). Earthquake source parameters determined by the SAFOD Pilot Hole seismic array. *Geophysical Research Letters, Vol. 31*, L12S09. doi:10.1029/2004GL019420.
Jaeger, J. C. (1971). Friction of rocks and stability of rock slopes. *Geotechnique, Vol. 21*, 97–134.
Jaeger, J. C., Cook, N. G. W., & Zimmermann, R. W. (2007). *Fundamentals of rock mechanics*. London: Blackwell Publishing.
Johnson, K. L. (1985). *Contact mechanics*. Cambridge: Cambridge University Press.
Johnson, L. R., & Nadeau, R. M. (2002). Asperity model of an earthquake: Static problem. *Bulletin of the Seismological Society of America, Vol. 92*, 672–686.
Kachanov, M. K., & Sevostianov, I. (2018). *Micromechanics of materials with applications*. Berlin: Springer-Verlag.
Kanwal, R. P. (1971). *Linear integral equations: Theory and technique*. New York: Academic Press.
Kassir, M. K., & Sih, G. C. (1975). *Three-dimensional crack problems: A new selection of crack problems in three-dimensional elasticity*. Leyden: Noordhoff International Publishing.
Kato, A., Igarashi, T., & Obara, K. (2014). Detection of a hidden Boso slow slip event immediately after the 2011 Mw 9 Tohoku-Oki earthquake, Japan. *Geophysical Research Letters, Vol. 41*, 5868–5874.
Kikuchi, N., & Oden, J. T. (1972). *Contact problems in elasticity. A study of variational inequalities and finite element methods*. Philadephia, PA: Studies in Applied and Numerical Mathematics, SIAM.
Kitajima, H., & Saffer, D. M. (2012). Elevated pore pressure and anomalously low stress in regions of low frequency earthquakes along the Nankai Trough. *Geophysical Research Letters, Vol. 39*, L23301.
Klarbring, A., Mikelić, A., & Shillor, M. (1991). The rigid punch problem with friction. *International Journal of Engineering Science, Vol. 29*, 751–768.
Kodaira, S., Likada, T., Kato, A., Park, J.-O., Iwasaki, T., & Kaneda, Y. (2004). High pore fluid pressure may cause silent slip in the Nankai Trough. *Science, Vol. 304*, 1295–1298.
Laursen, T. A. (2003). *Computational contact and impact mechanics*. Berlin: Springer-Verlag.
Linker, M. F., & Dieterich, J. H. (1992). Effects of variable normal stress on rock friction: observations and constitutive equations. *Journal of Geophysical Research (Solid Earth), Vol. 97*, 4923–4940.
Love, A. E. H. (1928). *A treatise on the mathematical theory of elasticity*. Oxford: Clarendon Press.
Luo, Y., & Ampuero, J.-P. (2018). Stability of faults with heterogeneous friction properties and effective normal stress. *Tectonophysics, Vol. 733*, 257–272.
Lur'e, A. I. (1964). Some *three-dimensional problems of the theory of elasticity*. *Wiley-Interscience, New York*.
Marone, C. (1998). Laboratory derived friction laws and their application to seismic faulting. *Annual Reviews- Earth and Planetary Science, Vol. 26*, 643–696.
Michalowski, R., & Mroz, Z. (1978). Associated and non-associated sliding rules in contact friction problems. *Archives of Mechanics, Vol. 30*, 259–276.
Michalowski, R. L., Zang, W., & Nadukuru, S. S. (2018). Maturing of contacts and ageing of silica sand. *Géotechnique, Vol. 68*, 132–145.
Mogi, K. (1974). On the pressure dependence of strength of rocks and the Coulomb fracture criterion. *Tectonophysics, Vol. 21*, 273–285.
Morris, J. P. (2003). *Review of rock joint models*. Livermore, CA: Lawrence Livermore laboratory Report.
Nadeau, R. M., & Johnson, L. R. (1998). Seismological studies at Parkfield IV. Moment release rates and estimates of source parameters for small repeating earthquakes. *Bulletin of the Seismological Society of America, Vol. 88*, 790–814.
Nadeau, R. M., & McEvilly, T. V. (1999). Fault slip rates at depth from recurrence intervals of repeating micro-earthquakes. *Science, Vol. 285*, 718–721.
Nguyen, T. S., & Selvadurai, A. P. S. (1998). A model for coupled mechanical and hydraulic behavior of a rock joint. *International Journal for Numerical and Analytical Methods in Geomechanics, Vol. 22*, 29–48.
Nur, A. (1972). Dilatancy, pore fluids and premonitory variations of t_s/t_p travel times. *Bulletin of the Seismological Society of America, Vol. 62*, 1217–1222.
Olssen, R., & Barton, N. (2001). An improved model for hydromechanical coupling during shearing of joints. *International Journal of Rock Mechanics and Mining Sciences, Vol. 38*, 317–329.
Panagiotopoulos, P. D. (1989). *Inequality problems in mechanics and applications. Convex and nonconvex energy functions*. Basel: Birkhauser-Verlag.
Pellet, F. L., & Selvadurai, A. P. S. (2016). *Rock damage mechanics, Chapter 3 in Rock Mechanics and Engineering* (pp. 65–107). Boca Raton, FL: CRC Press. (X.-T. Feng, Ed.).
Persson, B. J. N. (2000). *Sliding friction: Physical principles and applications*. Berlin: Springer-Verlag.
Pietruszczak, S. (2010). *Fundamentals of plasticity in geomechanics*: Vol. Fl. Boca Raton: CRC Press.
Plesha, M. E. (1987). Constitutive models for rock discontinuities with dilatancy and surface degradation. *International Journal for Numerical and Analytical Methods in Geomechanics, Vol. 11*, 345–362.
Plesha, M. E., & Belytschko, T. (1985). A constitutive operator splitting method for non-linear transient analysis. *International Journal for Numerical Methods in Engineering, Vol. 21*, 1729–1745.
Plesha, M. E., Ballarini, R., & Parulekar, A. (1989). Constitutive model and finite element procedure for dilatant contact problems. *Journal of the Engineering Mechanics Division Proc ASCE, Vol. 115*, 2649–2668.
Prasseyto, S. H., Guttierrez, M., & Barton, N. (2017). Nonlinear shear behavior of rock joints using a linearized implementation of the Barton-Bandis model. *Journal of Rock Mechanics and Geotechnical Engineering, Vol. 9*, 671–682.
Raous, M., Jean, M., & Moreau, J. J. (Eds.). (1995). *Contact mechanics*. New York: Plenum Press.
Rice, J. R. (1975). On the stability of dilatant hardening for saturated rock masses. *Journal of Geophysical Research, Vol. 80*, 1531–1536.
Rice, J. R., & Cocco, M. (2007). Seismic fault rheology and earthquake dynamics. In N. Holvus, G. Hirth, & M. R. Handy (Eds.), *Tectonic faults: Agents of change on a dynamic earth* (pp. 99–137). MA: MIT Press.
Rice, J. R., & Ruina, A. L. (1983). Stability of steady frictional slipping. *Journal of Applied Mechanics, Vol. 50*, 343–349.

Rice, J. R., Rudnicki, J. W., & Platt, J. D. (2014). Stability and localization of rapid shear in fluid-saturated gouge: 1. Linearized stability analysis. *Journal of Geophysical Research (Solid Earth), Vol. 119*, 4311–4333.
Rossmanith, H.-P. (1997). *Proceedings of the First International Conference on Damage and Failure of Interface*. Rotterdam: DFI-Vienna, AA Balkema.
Rudnicki, J. W., & Chen, C.-H. (1988). Stabilization of rapid frictional slip on a weakening fault by dilatant hardening. *Journal of Geophysical Research, Vol. 93*, 4745–4757.
Ruina, A. L. (1983). Slip instability and state variable friction laws. *Journal of Geophysical Research, Vol. 88*, 10359–10370.
Sammis, C. G., & Rice, J. R. (2001). Repeating earthquakes as Low-Stress-Drop Events at a border between locked and creeping fault patches. *Bulletin of the Seismological Society of America, Vol. 91*, 532–537.
Sammis, C. G., Nadeau, R., & Johnson, L. R. (1999). How strong is an asperity. *Journal of Geophysical Research (Solid Earth), Vol. 104*, 10609–10619.
Scholz, C. (1998). Earthquakes and friction laws. *Nature, Vol. 391*, 37–42.
Scholz, C. H. (2002). *The mechanics of earthquakes and faulting*. Cambridge: Cambridge University Press.
Scuderi, M. M., & Colletini, C. (2016). The role of fluid pressure in induced vs. triggered seismicity: Insights from rock deformation experiments on carbonates. *Scientific Reports, Vol. 6*, 24852.
Scuderi, M., Collettini, C., & Marone, C. (2017). Frictional stability and earthquake triggering during fluid pressure stimulation of an experimental fault. *Earth and Planetary Science Letters, Vol. 477*, 84–96.
Segall, P., & Lu, S. (2015). Injection-induced seismicity: poroelastic and earthquake nucleation effects. *Journal of Geophysical Research (Solid Earth), Vol. 120*, 5082–5103.
Selvadurai, A. P. S. (1979). *Elastic analysis of soil-foundation interaction, developments in geotechnical engineering*: Vol. 17. The Netherlands: Elsevier Scientific Publishing Co.
Selvadurai, A. P. S. (1980). Asymmetric displacements of a rigid disc inclusion embedded in a transversely isotropic elastic medium of infinite extent. *International Journal of Engineering Science, Vol. 18*, 979–986.
Selvadurai, A. P. S. (1985). On an integral equation governing an internally indented penny-shaped crack. *Mechanics Research Communications, Vol. 12*, 347–351.
Selvadurai, A. P. S. (1994a). Matrix crack extension at a frictionally constrained fiber. *Journal of Engineering Materials and Technology, Trans. ASME, Vol. 116*, 398–402.
Selvadurai, A. P. S. (1994b). Separation at a pre-fractured bi-material geological interface. *Mechanics Research Communications, Vol. 21*, 83–88.
Selvadurai, A. P. S. (1995). Boundary element modelling of geomaterial interfaces. In A. P. S. Selvadurai, & M. J. Boulon (Eds.), *Mechanics of geomaterial interfaces* (pp. 395–420). New York: Elsevier.
Selvadurai, A. P. S. (1999). In-plane loading of a rigid disc inclusion embedded in a crack. *International Journal of Solids and Structures, Vol. 36*, 1701–1714.
Selvadurai, A. P. S. (2000a). Fracture evolution during indentation of a brittle elastic solid. *Mechanics of Cohesive-Frictional Materials, Vol. 5*, 325–339.
Selvadurai, A. P. S. (2000b). Indentation of a pre-compressed penny-shaped crack. *International Journal of Engineering Science, Vol. 38*, 2095–2111.
Selvadurai, A. P. S. (2000c). Partial Differential Equations in Mechanics. *The biharmonic equation, Poisson's equation*: Vol. 2. Berlin: Springer-Verlag.
Selvadurai, A. P. S. (2003). On an invariance principle for unilateral contact at a bi-material elastic interface. *International Journal of Engineering Science, Vol. 41*, 721–739.
Selvadurai, A. P. S. (2006). Deflections of a rubber membrane. *Journal of the Mechanics and Physics of Solids, Vol. 54*, 1093–1119.
Selvadurai, A. P. S. (2015). Bridged defects in continuously and discretely reinforced solids. *Journal of Engineering Mathematics, Vol. 95*, 359–380.
Selvadurai, A. P. S. (2016). Indentation of a spherical cavity in an elastic body by a rigid spherical inclusion: influence of non-classical interface conditions. *Continuum Mechanics and Thermodynamics, Vol. 28*, 617–632.
Selvadurai, A. P. S. (2010). In S. N. Atluri (Ed.), *Contact mechanics in the engineering sciences. Material characterization, micromechanical processes and modelling geosciences* (pp. 395–420). GA: Tech Science Press.
Selvadurai, A. P. S., & Boulon, M. J. (Eds.) (1995). *Mechanics of Geomaterial Interfaces, Studies in Applied Mechanics* (Vol. 42). Amsterdam: Elsevier.
Selvadurai, A. P. S., & Katebi, A. (2015). An adhesive contact problem for an incompressible non-homogeneous elastic halfspace. *Acta Mechanica, Vol. 226*, 249–265.
Selvadurai, A. P. S., & Nguyen, T. S. (1999). Mechanics and fluid transport in a degradable discontinuity. *Engineering Geology, Vol. 53*, 243–249.
Selvadurai, A. P. S., & Singh, B. M. (1984). On the expansion of a penny-shaped crack by a rigid disc inclusion. *International Journal of Fracture, Vol. 25*, 69–77.
Selvadurai, A. P. S., & Singh, B. M. (1985). The annular crack problem for an isotropic elastic solid. *Quarterly Journal of Mechanics and Applied Mathematics, Vol. 38*, 233–243.
Selvadurai, A. P. S., & Suvorov, A. P. (2016). *Thermo-poroelasticity and geomechanics*. Cambridge: Cambridge University Press.
Selvadurai, A. P. S., & Voyiadjis, G. Z. (1986). Mechanics of Interfaces. *Studies in applied mechanics*: Vol. 11. Amsterdam: Elsevier.
Selvadurai, A. P. S., & Yu, Q. (2005). Mechanics of a discontinuity in a geomaterial. *Computers and Geotechnics, Vol. 32*, 92–106.
Selvadurai, A. P. S., & Yu, Q. (2006). On the indentation of a polymeric membrane. *Proceedings of the Royal Society, Ser A, Vol. 462*, 189–209.
Selvadurai, A. P. S., Suvorov, A. P., & Selvadurai, P. A. (2015). Thermo-hydro-mechanical processes in fractured rock formations during glacial advance. *Geoscientific Model Development, Vol. 8*, 2167–2185.
Selvadurai, P. A., & Glaser, S. D. (2015). Laboratory developed contact models controlling instability on frictional faults. *Journal of Geophysical Research (Solid Earth), Vol. 120*, 4208–4236.
Selvadurai, P. A., & Glaser, S. D. (2017). Asperity generation and its relationship to seismicity on a planar fault: a laboratory simulation. *Geophysical Journal International, Vol. 208*, 1009–1025.
Selvadurai, P. A., Edwards, B. E., Tormann, T., Wiemer, S., & Glaser, S. D. (2018). Characteristics of seismicity on worn faults-source dimensions of frictional precursory seismicity controlled by fault roughness (*in preparation*).
Sibson, R. H. (1992). Fault-valve behaviour and the hydrostatic-lithostatic fluid pressure interface. *Earth Science Reviews, Vol. 32*, 141–144.
Siman-Tov, S., Aharanov, E., Boneh, Y., & Reches, Z. (2015). Fault mirrors along carbonate faults: formation and destruction during shear experiments. *Earth and Planetary Science Letters, Vol. 430*, 367–376.
Sneddon, I. N. (1966). *Mixed boundary value problems in potential theory*. North-Holland, Amsterdam: Publishing Co.
Taylor, D. W. (1948). *Fundamentals of soil mechanics*. New York: John Wiley.
Tranter, C. J. (1960). Some triple integral equations. *Glasgow Mathematical Journal, Vol. 4*, 200–203.
Turrin, S., Hanss, M., & Selvadurai, A. P. S. (2009). An approach to uncertainty analysis of rockfall simulation. *Computer Modeling in Engineering and Sciences, Vol. 1350*, 1–22.
Ufliand, Ia. S. (1965). *Survey of applications of integral transforms in the theory of elasticity* (pp. 65–1556). Raleigh, NC: North Carolina State College. (Engl. Trans. Edited by IN Sneddon) Tech. Rep.
Villaggio, P. (1980). A unilateral contact problem in elasticity. *Journal of Elasticity, Vol. 10*, 113–119.
Wan, R., Nicot, F., & Darve, F. (2017). *Failure in geomaterials: A contemporary treatise*. Amsterdam: Elsevier Inc.
Williams, W. E. (1963). Integral equation formulation of some three-part boundary value problems. *Proceedings of the Edinburgh Mathematical Society, Vol. 13*, 317–323.
Willner, K. (2003). *Kontinuums- und Kontaktmechanik. Synthetische und analytische Darstellung*. Berlin: Springer-Verlag.
Wriggers, P., & Laursen, T. A. (2007). *Computational contact mechanics*. Berlin: Springer-Verlag.
Zang, A., & Stephansson, O. (2010). *Stress field of the earth's crust*. Berlin: Springer-Verlag.
Zienkiewicz, O. C., Best, B., Dullage, C., & Stagg, K. G. (1970). Analysis of nonlinear problems in rock mechanics with particular reference to jointed rock systems. In *Proceedings 2nd Congress of the International Society for Rock Mechanics: Vol. 2* (pp. 501–509).